Transportation Research Part B 113 (2018) 121–142

Contents lists available at ScienceDirect

Transportation Research Part B

journal homepage: www.elsevier.com/locate/trb

Travel time estimation by urgent-gentle class traffic flow model

Yongliang Zhang[a], M.N. Smirnova[b,*], A.I. Bogdanova[b], Zuojin Zhu[a,b,*], N.N. Smirnov[b,c]

[a] Faculty of Engineering Science, USTC, Hefei, 230026, China
[b] Faculty of Mechanics and Mathematics, LMSU, Moscow, Russia
[c] Scientific Research Institute for System Analysis, Russian Academy of Sciences, Moscow, Russia

ARTICLE INFO

Article history:
Received 15 October 2017
Revised 15 May 2018
Accepted 15 May 2018

Keywords:
Urgent density fraction
Travel time
Local average speed
Spatial-temporal evolutions

ABSTRACT

To estimate travel time through a ring road, an urgent-gentle class traffic flow model (UGM) with viscoelastic and ramp effects is developed. Vehicles in traffic flow are divided into urgent and gentle categories, and the urgent class has the demand of arriving at destination in time, while the gentle class hasn't. It is assumed that the urgent and gentle classes have the same instantaneous speed to simply the mathematical modeling. To validate the proposed traffic model, a Navier–Stokes like model (Zhang, 2003) is further extended just for validating the present model. Numerical simulations based on the present model are carried out to calculate the travel time on a ring road with total length of 80 km and four initially assumed jams. It was found that similar to the effect of initially assumed jams, the on/off ramp flows play significant roles in the formation and evolution of traffic flow patterns. Urgent density fraction propagates at local traffic speed, its temporal evolution and spatial distribution curves have different shapes as compared with that of traffic density and speed. The average travel time increases monotonically with the increase of ring road initial density. Rational management of road operation is necessary.

1. Introduction

Traffic flows have been widely studied due to the significant impacts on travel time and economic activities. Therefore, to explore characteristics and properties of traffic flows, many macroscopic traffic models have been developed, among which is the well-known model LWR (Lighthill and Whitham, 1955; Richards, 1956), the Euler model (Payne, 1971), the gas-kinetic-based model (Helbing and Treiber, 1998; Hoogendoorn and Bovy, 2000), the Navier–Stokes like model (Kerner and Konhäuser, 1993), and the generic model (Lebacque et al., 2007; Lebacque and Khoshyaran, 2013).

A conserved higher-order anisotropic traffic flow model was developed by introducing a pseudo-density transformed from the velocity, with traffic pressure taken as a function of the pseudo-density and the relaxation of velocity to equilibrium (Zhang et al., 2009). The model has certainly provided a fresh point of view for traffic flow modeling, however its potential of application needs further studies. For instance, how to assign the value of the so-called pseudo-density, and how to choose the density-velocity relationship as well as its corresponding effects.

* Corresponding authors.
E-mail addresses: wonrims@inbox.ru (M.N. Smirnova), zuojin@ustc.edu.cn (Z. Zhu).

https://doi.org/10.1016/j.trb.2018.05.010
0191-2615/

Traffic flow pattern formation phenomena in traffic systems have a spectrum surprisingly rich. These phenomena can be described by the car-following models, the cellular automaton models (Nagel and Schreckenberg, 1992; Helbing and Huberman, 1998; Chowdhury et al., 2000), the gas-kinetic models or the fluid-dynamical models (Nagatani, 2002). Some traffic flow questions have been answered (Helbing, 2001).

Using the gas-kinetic based approach (Ngoduy, 2012), a macroscopic model was developed (Ngoduy, 2013) to describe the traffic flow where intelligent vehicles are moving closer to each other than manual vehicles and operating in a form of many platoons each of which contains several vehicles. A stochastic conservative model in continuous time over discrete space, following a misanthrope Markovian process was studied (Tordeux et al., 2014). Generic second order modeling (GSOM) family can be expressed as a system of conservation laws; for models of the GSOM family, an adequate framework for effective numerical methods was obtained (Costeseque and Lebacque, 2014).

A new formula of non-equilibrium traffic flow models based on their isomorphic relation with optimal control problems was given (Li and Zhang, 2013). With the formula, generic initial-boundary conditions can be easily handled and a simplified numerical solution scheme for non-equilibrium traffic flow models can be devised.

In recent years, in analogy to non-Newtonian fluid flow, viscoelastic traffic modeling has been carried out to develop macroscopic continuum models (Zhu and Yang, 2013; Bogdanova et al., 2015), for which the sensitivity of traffic flow to viscoelasticity has been explored recently (Smirnova et al., 2016; Smirnova et al., 2017).

For travel time prediction, Chang and Mahmassani (1988) examined two heuristic rules, which are proposed for describing urban commuters' predictions of travel time as well as the adjustments of departure time in response to unacceptable arrivals in their daily commute under limited information. Based on the notion, they found the magnitude of the predicted travel time depends on each commuter's own experience, including recallable travel time, schedule delay, and difficulties in searching for a satisfactory departure time. To estimate travel time, Dailey (1993) demonstrated the viability of using cross-correlation techniques with inductance loop data to measure the propagation time of traffic. An improved algorithm for estimating travel time with dual loop detectors was reported by Lint and der Zijpp (2003). The travel time prediction results and accuracy generated by different prediction models were discussed by Chien and Kuchipudi (2003).

For travel-time prediction, support vector regression (SVR) was applied (Wu et al., 2004). In comparison its results to other baseline travel-time prediction methods using real freeway traffic data, it was found that the SVR predictor can significantly reduce both relative mean errors and root-mean-squared errors of predicted travel times.

A freeway travel time prediction framework was reported (van Lint et al., 2005), it exploits a recurrent neural network topology, the so-called state space neural network (SSNN) has preprocessing strategies based on imputation. The SSNN model is based on the lay-out of the freeway stretch of interest, can yield good accurate and robust travel time predictions on both synthetic and real data.

To predict arterial traffic conditions using streaming GPS (global positioning system) probe data, a hybrid modeling framework was proposed (Hofleitner et al., 2012). The model is based on a well-established theory of traffic flow through signalized intersections and is combined with a machine learning framework to both learn static parameters of the roadways (such as free flow velocity or traffic signal parameters) as well as to estimate and predict travel times through the arterial network. It was indicated that this approach is a significant step forward in estimating traffic states throughout the arterial network using a relatively small amount of real-time data.

To estimate arterial route travel time distribution, a Markov chain technique was presented (Ramezani and Geroliminis, 2012). Given probe vehicles travel times of the traversing links, in the technique a two-dimensional (2D) diagram was established with data points representing travel times of a probe vehicle crossing two consecutive links. To cluster each 2D diagram to rectangular sub spaces (states) with regard to travel time homogeneity, a heuristic grid clustering method was developed. It was found that the results are very close to the Markov chain procedure and more accurate once compared to the convolution of links travel time distributions for different levels of congestion, even for small penetration rates of probe vehicles.

For urban road network travel time estimation, Jenelius and Koutsopoulos (2013) presented a model using vehicle trajectories obtained from low frequency GPS probes as observations, where the vehicles typically cover multiple network links between reports. The network model separates trip travel times into link travel times and intersection delays, allows correlation between travel times on different network links based on a spatial moving average (SMA) structure. The potential of using sparse probe vehicle data for monitoring the performance of the urban transport system was highlighted by case study.

To predict experienced travel time for congested freeways, a methodological framework was developed (Yildirimoglu and Geroliminis, 2013). The method sequentially includes a bottleneck identification algorithm, clustering of traffic data in traffic regimes with similar characteristics, development of stochastic congestion maps for clustered data and an online congestion search algorithm, which combines historical data analysis and real-time data to predict experienced travel times at the starting time of the trip. It was found that the proposed method provides promising travel time predictions under varying traffic conditions.

For travel time estimation on urban arterials, variational theory was applied (Hans et al., 2015). It was reported that the LWR model can be expressed as a least cost path problem, which can be simply applied on a graph with a minimal number of nodes and edges when the fundamental diagram is triangular (sufficient variational graph– SVG); described how to obtain a tight estimation of the arterial capacity by properly identifying the most constraining part of the SVG, found that a modified version of the SVG allows the exact calculation of the cumulative count curves at the entry and exit of an arterial, and it is finally possible to derive the full travel time distributions for any dynamic conditions.

More recently, Kumar et al. (2017) developed a bus travel time prediction method that considers both temporal and spatial variations in travel time, where the governing equations for traffic density and speed are solved. It was found that the proposed approach is good enough for the considered application of bus travel time prediction. To address the problem of dynamic travel time forecasting within highway traffic networks using speed measurements, Ladino et al. (2017) presented definitions, computational details and properties in the construction of dynamic travel time, which was dynamically clustered using a K-means algorithm. The algorithm was deployed in a real time application and the performance was evaluated using real traffic data from the South Ring of the Grenoble city in France.

To estimate the probability distribution of trip travel times from link travel time distributions and takes into consideration correlations in time and space, Ma et al. (2017) proposed a generalized Markov chain approach, which consists of three major components, namely state definition, transition probabilities estimation and probability distribution estimation. To predict urban network link travel times from sparse floating car data (FCD), it usually needs pre-processing, mainly map-matching and path inference. Hence, a fixed point formulation was proposed to describe the simultaneous path inference and travel time estimation problem (Rahmani et al., 2017). It was shown that standard fixed point iterations converge quickly to a solution where input and output travel times are consistent.

In this paper, by dividing vehicles into urgent and gentle classes, and further including traffic viscoelastic effect and ramp influence, in order to estimate travel time on ring road, an urgent-gentle class traffic flow model (UGM) is developed. In the UGM, an expression of traffic pressure is derived by postulating that it is proportional to the reciprocal of space headway. Measured by the jam density and the free flow speed of gentle class, a special curve for traffic pressure is obtained. Traffic sound speed is rigorously derived from the definition in classical mechanics. Measured by the sound speed defined at the second critical point, the sound speed curve is illustrated. The vehicular driving behaviors are distinguished by free flow speed and braking distance, urgent class generally attempts to its destination as early as possible, should have larger free flow speed and braking distance. Braking distance is generally a function of free flow speed (Kiselev et al., 2000).

To validate the traffic model, using the same expressions for traffic pressure and traffic sound speed in UGM, the extended Navier–Stokes like model developed by Zhang (2003) has been extended and named EZM (extended Zhang's model), which is then used to explore the application potential of the present UGM, and estimate the travel time through a ring road with total length 80 km numerically.

By preassigning a distinguishing- time period to calculate the local average speed, named Δ_0, we will give expressions for estimating the travel time and its root mean square value. This paper introduces the UGM and a TVD (total variation diminishing) based numerical method just before describing EZM, arranges the section of parameters and conditions just before the section of results and discussion, and finally gives the conclusions.

2. Urgent-gentle class traffic model

To seek traffic flow characteristics with different driving behaviors, we develop an urgent-gentle class traffic model, which divides vehicles into double classes: urgent, and gentle. The urgent class has a higher free flow speed and a larger braking distance to fulfill the demand of arriving at destination in time, while the gentle class doesn't have.

For simplicity, we assume: (i) urgent class has the same speed as gentle class, but has different free flow speed and braking distance. (ii) traffic flow satisfies a linear viscoelastic constitutive relation; (iii) ramp flow effect is permitted. The 1st assumption is used to simplify the momentum conservation form of traffic flow. The 2nd assumption allows the use of visco-elastic traffic model for single class vehicles, as reported recently (Zhu and Yang, 2013; Bogdanova et al., 2015). Labeling urgent density and gentle density of traffic flow by ρ_1 and ρ_2 respectively, taking total traffic density $\rho(=\rho_1+\rho_2)$, urgent density fraction $s(=\rho_1/\rho)$ and traffic flow speed $q=\rho u$ as mandatory variables, the UGM can be described in the form

$$\begin{cases}\rho_t+q_x=\sigma_1 q,\\ \rho(u_t+uu_x)=R,\\ (s\rho)_t+(sq)_x=s\sigma_2 q.\end{cases} \tag{1}$$

where R satisfies the expression (Bogdanova et al., 2015)

$$R=\rho(u_e-u)/\tau-p_x+[(2G\tau)u_x]_x, \tag{2}$$

here p is traffic pressure, u_e is equilibrium traffic speed obtained by fundamental diagram as shown in Fig. 1, R/ρ represents traffic flow acceleration, with G and τ denoting modulus of vehicular fluid elasticity and relaxation time of traffic flow respectively. As the kinematic viscosity of traffic flows can be defined by $\nu=2G\tau/\rho$ (Bogdanova et al., 2015), it means that the modulus of traffic elasticity G is inversely proportional to the relaxation time τ. When the road is empty, the modulus G is zero. The term $[(2G\tau)u_x]_x$ in Eq. (2) reflects some properties of traffic self-organization. Any increase of speed ahead of a vehicle, which inclines to generate a positive value for second spatial derivative of speed u_{xx}, provides the drivers' motivation for acceleration, because in congested traffic flows the reduction of density ahead of the vehicle can be foreseen.

It is noted to describe ramp flow effect, variables based random number generator with Gaussian normal distribution, such as σ_1 and σ_2, are introduced. When local traffic flow flux q is zero, the source terms caused by ramp flows should

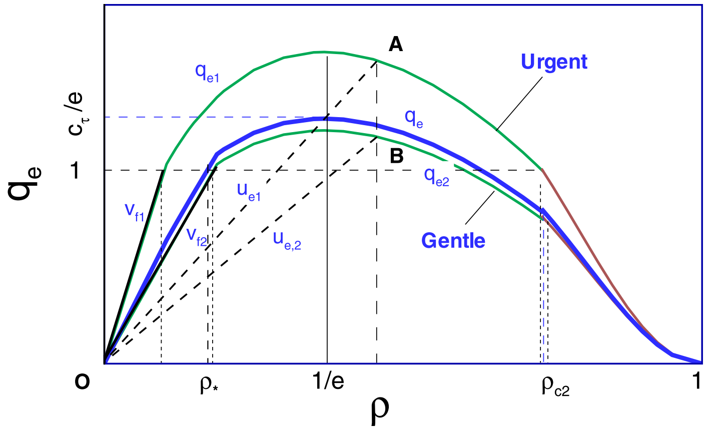

Fig. 1. Fundamental diagram for urgent-gentle class traffic flows. Note that ρ is measured by jam density ρ_m.

vanish, which is naturally true at off-ramp cross-sections. While at on-ramp cross-sections, the on-ramp flow is generally less than the flow on the main road, implying the random variables should have values less than unity.

Eq. (1) indicates the gentle density $\rho_2 = (1-s)\rho$ satisfies

$$[(1-s)\rho]_t + [(1-s)q]_x = (\sigma_1 - s\sigma_2)q,$$

which means that its right hand term can be simply written as $(1-s)\sigma_2 q$ if we take $\sigma_1 = \sigma_2$.

As urgent and gentle classes vehicles have different free flow speed and braking distance, the equilibrium speeds of traffic flow for the urgent and gentle classes are also different, as shown in fundamental diagram Fig. 1, labeling the jam density by ρ_m, the equilibrium speed can be written as

$$u_{ej} = \begin{cases} v_{fj}, & \text{for } \rho \le \rho_{*j}; \\ -c_{\tau j}\ln(\rho/\rho_m), & \text{for } \rho_{*j} < \rho \le \rho_{c2j}; \\ B_j\{1 - \operatorname{sech}[\Lambda_j \ln(\rho/\rho_m)]\}, & \text{for } \rho_{c2} < \rho \le \rho_m. \end{cases} \tag{3}$$

At second critical density ρ_{c2}, traffic flow has an equilibrium speed u_{c2}. When the speed is used to define a ratio $\Lambda_j = c_{\tau j}/u_{c2}$, the parameter B_j can be written as

$$B_j = u_{c2}/\{1 - \operatorname{sech}[\Lambda_j \ln(\rho_{c2j}/\rho_m)]\}. \tag{4}$$

Labeling by subscript 'j' for some variables of fully urgent ($j = 1$) and fully gentle ($j = 2$) traffic flows respectively, then at any urgent density fraction s, the equilibrium speed u_e and relaxation time τ for mixed traffic can be written as

$$\begin{cases} u_e = u_{e2} + (u_{e1} - u_{e2})s; \\ \tau = \tau_2 + (\tau_1 - \tau_2)s; \\ c_\tau = c_{\tau 2} + (c_{\tau 1} - c_{\tau 2})s. \end{cases} \tag{5}$$

with the 1st critical density ρ_* and 2nd critical density ρ_{c2} given by

$$\begin{cases} \rho_* = \rho_{*2} + (\rho_{*1} - \rho_{*2})s; \\ \rho_{c2} = \rho_{c22} + (\rho_{c21} - \rho_{c22})s. \end{cases} \tag{6}$$

The equilibrium speed-density relation relevant to the three situations described by Eq. (3) is assumed with respect to the existence of second critical phenomenon observed in traffic flows.

As reported Bogdanova et al. (2015), traffic pressure p is proportional to the reciprocal of spatial headway, it can be defined by

$$p = K \cdot \{\rho/[1 - \alpha(\rho/\rho_m)]\}. \tag{7}$$

where $\alpha = l\rho_m$, l is the average length of vehicles, and K is a parameter of traffic pressure modeling. This pressure definition to a certain extent is reasonable, as the spatial headway $[1/\rho - l]$ tends to zero, the pressure approaches to infinity, generating a strong stoppage demand for vehicles. The Definition (7) also indicates that the traffic pressure grows with the increase of density monotonically, but the growth rate is more rapidly when traffic flow state approaches to the completely jammed condition.

It is noted that the traffic acceleration R/ρ depends on pressure gradient p_x/ρ, implying possible occurrences of negative speeds in the solutions, even in the cases of excluding the viscous and relaxation time related terms, as reported by Aw and Rascle (2000). As a car is an anisotropic particle that mostly responds to frontal stimuli, not completely identical to a fluid particle, in the mathematical modeling of vehicular acceleration, relaxation time related term $\rho(u_e - u)/\tau$ should be included. By following the *principle* that all traffic waves connecting any state to its left must have a propagation speed (shock speed) *at most* equal to the traffic speed, anisotropic higher-order traffic flow models have been developed and studied (Rascle, 2002; Xu et al., 2007).

In the present UGM, the use of traffic pressure gradient leads to the *principle* for shock speed mentioned above not been adhered. The use of the term $\rho(u_e - u)/\tau$ can decrease the probability of negative speed occurrences, in particular when geometric average of $2G\tau$ is used to set the visco-elasticity on the mesh-faces, such as in the numerical simulation of a queue-stoppage at a traffic light with models that have abandoned the *principle* for shock speed.

Using its definition in classical mechanics, the sound speed of traffic flow at constant entropy should be

$$c = \sqrt{\frac{\partial p}{\partial \rho}} = K^{1/2}/(1 - \alpha\rho/\rho_m), \tag{8}$$

it denotes the propagation speed of infinitesimal disturbances, which can be used to describe the propagation speeds of traffic waves, such as the deceleration wave propagation in the upstream direction, and the packing wave propagation established in the downstream direction (Kiselev et al., 2000). If we assume the sound speed of traffic flow at second critical density is just-right identical to c_τ (Ma et al., 2017), an explicit expression for K is

$$K = c_\tau^2(1 - \alpha\rho_{c2}/\rho_m)^2. \tag{9}$$

The assumption for sound speed at second density is made with regard to the previous work of Kiselev et al. (2000). It was reported that when the free flow speed is 80 km/h, relevant to the braking distance 45 m and average length of vehicles 5 m, the value of c_τ is about 35 km/h, which is close to the experimental data from traffic observations in the Lincoln Tunnel in New York used in the traffic flow analysis of Whitham (1974).

To describe τ explicitly, supposing $(c \cdot \tau) =$ Const, and denoting relaxation time at ρ_{c2} by $\tau_0 = l_0/c_\tau$ with traffic length scale l_0, we have (Bogdanova et al., 2015)

$$\begin{aligned} c/c_0 &= \tau_0/\tau, \\ &= (1 - \alpha\rho_{c2}/\rho_m)/(1 - \alpha\rho/\rho_m). \end{aligned} \tag{10}$$

Here $c_0 = c_\tau$ at second critical density ρ_{c2}. Obviously, the relaxation time τ decreases linearly with traffic density. For the urgent-gentle class traffic flows, the relaxation time τ_0 estimated by length scale l_0, is also dependent on the urgent density fraction s, but not a constant.

Denoting the braking distances for urgent and gentle classes by X_{br1} and X_{br2} respectively, the corresponding maximum permissible density ρ_{*j} at free flow speed v_{fj} is

$$\rho_{*j} = \rho_m \exp(-v_{fj}/c_{\tau j}). \tag{11}$$

As safe traffic density (ρ_{*j}) itself implies that the distance between vehicles are not shorter than the braking distance X_{brj}, denoting average vehicle length by l, then ρ_{*j} is defined by

$$\rho_{*j} = \rho_m[1 + X_{\text{brj}}/l]^{-1}, \tag{12}$$

which is generally referred to as 1st critical density or 1st transitional density. Combining Eq. (11) and Eq. (12), we obtain

$$c_{\tau j} = v_{fj}/\ln[1 + X_{\text{brj}}/l]. \tag{13}$$

It is noted that c_τ for single class regular traffic has been used as propagation speed of disturbances in the analysis of Kiselev et al. (2000).

To describe the mandatory variables ρ, q and s in urgent-gentle class traffic flows, in addition to random variables σ_1 and σ_2 introduced to describe ramp flow effect, other parameters defined by the UGM are

$$\begin{cases} \tau, & \text{relaxation time, s;} \\ G, & \text{modulus of vehicular fluid elasticity, veh} \cdot \text{m/s}^2; \\ u_e, & \text{equilibrium speed, m/s;} \\ p, & \text{traffic pressure, veh} \cdot \text{m/s}^2. \end{cases}$$

The product of the modulus G and relaxation time τ is just a half of dynamic viscosity, i.e. $G\tau = \frac{1}{2}\rho\nu$. The equilibrium speed $u_e = u_{e2} + (u_{e1} - u_{e2})s$, depends linearly on the urgent density fraction s, with its value determined by the fundamental diagram shown in Fig. 1. The parameters v_{fj}, $c_{\tau j}$, and B_j are used to describe the equilibrium speed u_{ej} of class-j in Eq. (3). As expressed by Eq. (7), the traffic pressure p is derived by assuming that it is proportional to the reciprocal of spatial headway.

The UGM described by Eq. (1) is employed to predict travel time passing through the ring road with ramp effect (schematically shown in Fig. 2) by numerical simulation. The model of Zhang (2003) is also at first extended for the double-class traffic flows and then used to provide numerical results for comparison.

It is noted one advantage of the traffic flow model is that the eigenvalues of Jacobian matrix can be derived more rapidly than the multi-class traffic model discussed in Refs. Zhu et al. (2004) and Xie et al. (2006).

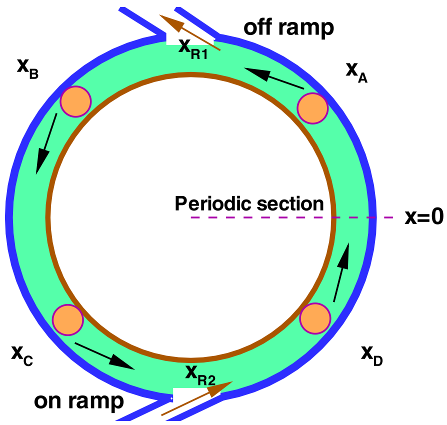

Fig. 2. Schematic diagram of ring traffic flow with four initial jams located at $X_I(I = A,\ B,\ C,\ D)$.

3. Numerical method

The numerical method for solving the UGM is based on total variation diminishing (TVD), which is a property of certain discretization schemes used to solve hyperbolic partial differential equations. The TVD- based schemes are able to capture shocks and avoid numerical oscillations.

Using definition $\partial p/\partial\rho = c^2$ and $p_x = c^2\rho_x$, by taking $R_1 = R + p_x + \sigma_1 q\cdot u$ instead of R, the governing Eqs. (1) and (2) become

$$\frac{\partial \mathbf{U}}{\partial t} + \frac{\partial \mathbf{F}(\mathbf{U})}{\partial x} = \mathbf{S}, \tag{14}$$

where $\mathbf{U} = (\rho, q, \rho_1)^T$, $\mathbf{F}(\mathbf{U}) = (q, q^2/\rho + p, \rho_1\cdot q/\rho)^T$, and $\mathbf{S} = (\sigma_1 q, R_1, \sigma_2 qs)^T$, with superscript 'T' representing vector transpose.

The eigenvalues of Eq. (14) λ_k, $(k = 1, 2, 3)$ may be expressed as $\lambda_1 = u - c$, $\lambda_2 = u + c$, and $\lambda_3 = u$, where the Jacobian matrix is

$$\mathbf{A} = \begin{pmatrix} \frac{\partial F_1}{\partial U_1} & \frac{\partial F_1}{\partial U_2} & \frac{\partial F_1}{\partial U_3} \\ \frac{\partial F_2}{\partial U_1} & \frac{\partial F_2}{\partial U_2} & \frac{\partial F_2}{\partial U_3} \\ \frac{\partial F_3}{\partial U_1} & \frac{\partial F_3}{\partial U_2} & \frac{\partial F_3}{\partial U_3} \end{pmatrix} = \begin{pmatrix} 0 & 1 & 0 \\ -u^2 + c^2 & 2u & 0 \\ -\frac{uU_3}{U_1} & \frac{U_3}{U_1} & u \end{pmatrix}. \tag{15}$$

While some believe that the eigenvalue should not exceed the traffic speed, the present UGM uses non-Newtonian fluid flow analogy, such that the traffic speed involves vehicular cluster rather than a single car, the eigenvalue limit is irrelevant, as in fact an eigenvalue represents a propagation speed of traffic wave.

Total variation diminishing (TVD) scheme developed by Roe (1981) is adopted to find numerical solutions of governing Eq. (14). Denoting respectively the mesh size and ratio of time step to mesh size respectively by Δx_i and $\omega = \Delta t/\Delta x$, the Courant–Friedrichs–Lewy (CFL) condition of TVD is satisfied by

$$\omega = C_{\rm FL}/\max|\lambda_{k,i+1/2}|, \quad k = 1, 2, 3; \quad i = 0, 1, 2, \ldots, I_{\max} - 1, \tag{16}$$

where $\lambda_{k,i+1/2}$ represents the kth eigenvalue for $\mathbf{A}$ at $x_{i+1/2}$, $I_{\max}$ is the maximum number of mesh, and the Courant number $C_{\rm FL} = 0.4$ (Shui, 1998) is fixed in the numerical tests.

The source term $S_2(= R_1)$ is calculated at the time level t^n with a linear expansion of

$$R_1^{n+1/2} = R_1^n + \frac{1}{2}\left(\frac{\partial R_1}{\partial \rho}\right)\delta\rho^n + \frac{1}{2}\left(\frac{\partial R_1}{\partial q}\right)\delta q^n + \frac{1}{2}\left(\frac{\partial R_1}{\partial \rho_1}\right)\delta\rho_1^n, \tag{17}$$

where $\delta\rho^n = \rho^{n+1} - \rho^n$, $\delta q^n = q^{n+1} - q^n$, and $\delta\rho_1^n = \rho_1^{n+1} - \rho_1^n$. Representing the speed and length scales respectively by v_0 and $\Delta x(=l_0)$, where $v_0 = q_0/\rho_m = \rho_{*2}v_{f2}$, with ρ_{*2} and v_{f2} having values as shown in Table 1, we have time scale $t_0 = l_0/v_0$. For simplicity, using scaled variables as the same as unscaled, so that the dimensionless expression

$$\begin{aligned} R_1 &= R + c^2\rho_x + \sigma_1 q\cdot u \\ &= (q_e - q)/\tau + [(2G\tau)u_x]_x + \sigma_1 q\cdot u \end{aligned}$$

Table 1
Parameters of traffic flow on ring road.

L(km)	ρ_m (veh/km)	v_{f1} (km/h)	X_{br1} (m)	v_{f2} (km/h)	X_{br2} (m)
80	172	100	60	80	45
l (m)	l_0 (m)	$\sigma_{1\mathrm{av}}$	$\sigma_{2\mathrm{av}}$	Λ_1	Λ_2
5.8	100	0.1	0.05	1.980	2.458
ρ_{*1}	ρ_{*2}	ρ_{c21}	ρ_{c22}[a]	τ_{01} (s)	τ_{02}(s)
0.0676	0.114	0.6034	0.666	8.082	9.765
X_{R1}(km)	X_{R2}(km)	X_A (km)	X_B (km)	X_C(km)	X_D(km)
20	60	10	30	50	70

[a] ρ_{*1}, ρ_{c21}, ρ_{*2}, ρ_{c22} are measured by ρ_m, relevant to X_{br1} and X_{br2} respectively.

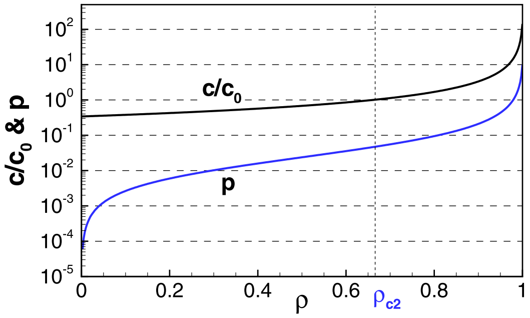

Fig. 3. Sound speed ratio c/c_0 and traffic pressure p versus density ρ, where ρ is measured by jam density ρ_m, with p measured by $\rho_m v_{f2}^2$.

keep the form unchanged, by simply neglecting the roles of viscous term $[(2G\tau)u_x]_x$ in the linear expansion, as the term $[(2G\tau)u_x]_x$ is just used to reflect certain properties of traffic self-organization and not dominant in the respect of numerical stability, we have

$$\begin{cases} \frac{\partial R_1}{\partial \rho} & = \sigma_1 u^2 + \tau^{-1}\left(\frac{\partial q_e}{\partial \rho}\right) - \frac{q_e - q}{\tau^2} \cdot \frac{\partial \tau}{\partial \rho}; \\ \frac{\partial R_1}{\partial q} & = 2\sigma_1 u - \tau^{-1} - \frac{q_e - q}{\tau^2} \cdot \frac{\partial \tau}{\partial q}; \\ \frac{\partial R_1}{\partial \rho_1} & = \tau^{-1}\left(\frac{\partial q_e}{\partial \rho_1}\right) - \frac{q_e - q}{\tau^2} \cdot \frac{\partial \tau}{\partial \rho_1}. \end{cases} \tag{18}$$

Considering $S_1 = \sigma_1 q$, $S_3 = \sigma_2 qs$, and $s = \rho_1/\rho$, we have

$$\frac{\partial S_1}{\partial \rho} = 0, \quad \frac{\partial S_1}{\partial q} = \sigma_1, \quad \frac{\partial S_1}{\partial \rho_1} = 0, \tag{19}$$

and

$$\frac{\partial S_3}{\partial \rho} = -\frac{\sigma_2 qs}{\rho}, \quad \frac{\partial S_3}{\partial q} = \sigma_2\ s, \quad \frac{\partial S_3}{\partial \rho_1} = \frac{\sigma_2 q}{\rho}. \tag{20}$$

Similarly, the source terms S_1 and S_3 can be calculated by

$$\begin{cases} S_1^{n+1/2} = S_1^n + \frac{1}{2}\left(\frac{\partial S_1}{\partial q}\right)\delta q^n, \\ S_3^{n+1/2} = S_3^n + \frac{1}{2}\left(\frac{\partial S_3}{\partial \rho}\right)\delta \rho^n + \frac{1}{2}\left(\frac{\partial S_3}{\partial q}\right)\delta q^n + \frac{1}{2}\left(\frac{\delta S_3}{\partial \rho_1}\right)\delta \rho_1^n. \end{cases} \tag{21}$$

The linearization procedures for of the source terms R_1, S_1 and S_3 are used to improve the temporal discretization accuracy of Eq. (14), and to increase the numerical stability of the TVD scheme, which has the form

$$\delta \mathbf{U}_i^n = -\omega(\hat{\mathbf{F}}_{i+1/2} - \hat{\mathbf{F}}_{i+1/2}) + (\Delta t)\mathbf{S}_i^n + \frac{\Delta t}{2}\left(\frac{\partial \mathbf{S}}{\partial \mathbf{U}}\right)_i^n \delta \mathbf{U}_i^n, \tag{22}$$

where $\delta \mathbf{U}_i^n = \mathbf{U}_i^{n+1} - \mathbf{U}_i^n$, $\Delta t (= t^{n+1} - t^n)$. The numerical flux $\hat{\mathbf{F}}_{i+1/2}$ can be calculated using the eigenvectors of Jacobian matrix A. The calculation of $\hat{\mathbf{F}}_{i+1/2}$ involves evaluating the coefficients of viscous term $Q_k(z)$ with an artificial parameter ϵ_k, as outlined by Zhu and Wu (2003) and Chang and Zhu (2006).

The traffic density dependence of traffic pressure p and sound speed ratio c/c_0 as shown in Fig. 3 is calculated so that they can then be used by linear interpolation in numerical tests. This approach in coding flow simulator is more flexible than directly utilizing explicit expressions of traffic pressure p and sound speed ratio c/c_0, therefore having a wider potential in applications.

For a special case of normalized initial density $\rho_0/\rho_m = 0.368$ [which will be simply written as ρ_0 in Eq. (26)], the evolutions of σ_1 and $\sigma_1 q$ can be seen in Fig. 4(a), with that of σ_2 and $\sigma_2 q$ shown in Fig. 4(b). The instant data of σ_1 and

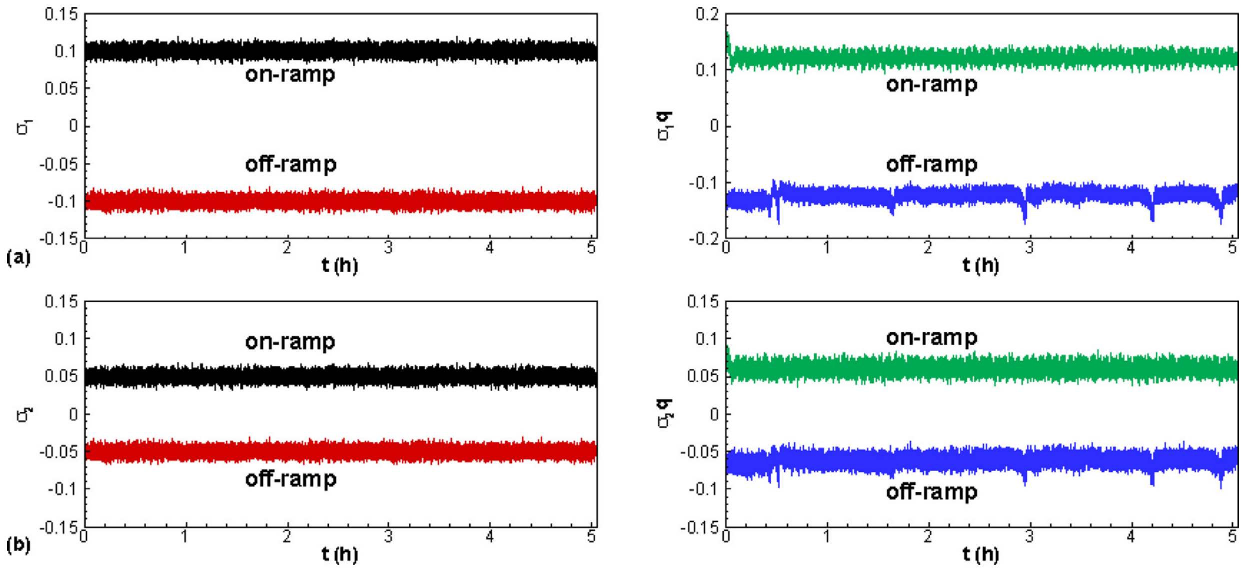

Fig. 4. (a) σ_1 and $\sigma_1 q$ versus time; (b) σ_2 and $\sigma_2 q$ versus time.

σ_2 measured by $1/l_0$, are calculated by random generator on the basis of Gaussian normal distribution. The data are recorded during the traffic flow simulation, which supposes that the ramp flow is randomly related to the local instantaneous main road flow at the ramp intersections at X_{R1} and X_{R2}. In Fig. 4(a), for the black curve, the mean value σ_1 for on-ramp at X_{R2} =600 is 0.1, but for the red curve at X_{R1}= 200 for off-ramp, it is set as −0.1. Taking the plus or minus symbol as on or off-ramp, the mean value $\sigma_{1\text{av}}$ is 0.1, with its root mean square value σ_1' equal to 0.005. From Fig. 4(b), it can be seen that $\sigma_{2\text{av}} = 0.05$, with σ_2'=0.005. The right part in Fig. 4 shows the recorded data of $\sigma_1 q$ and $\sigma_2 q$ in the simulation of ring traffic flow with initial density $\rho_0 = 0.368$, where unit of q is q_0, as shown in Fig. 1.

It is noted that the instantaneous value of σ_1 is predicted by a random generator with the artificially pre-assigned mean values of $\sigma_{1\text{av}}$ and σ_1', and so is for the instantaneous value of σ_2. In real operation systems, ramp flows do have intrinsic uncertainties. In the present work, the ramp flows are dealt with an assumption-based simple approach. To achieve the ramp flow characteristics in details, more theoretical and observation researches are needed.

4. Model for validation

To validate the reliability and applicability of the UGM described above, the traffic flow model derived by car-following rule (Zhang, 2003) is used. By assuming $\tau_0/\tau = c/c_0$, and $l_0 = c_0\tau_0$ similar to the work of Smirnova et al. (2017), the extended Zhang's model (EZM) can be written in the form

$$\begin{cases} \rho_t + q_x = \sigma_1 q, \\ q_t + \{q^2/\rho + p + [(2\beta c_0)\cdot(c/c_0)](q/\rho)\}_x = R, \\ (s\rho)_t + (sq)_x = \sigma_2 qs, \end{cases} \tag{23}$$

with

$$R = \left[\frac{(q_e - q)}{\tau_0}\right](c/c_0) + [(2\beta c_0)\cdot(c/c_0)\rho](q/\rho)_{xx} + (q/\rho)[(2\beta c_0)\cdot(c/c_0)\rho]_x, \tag{24}$$

where equilibrium flow rate $q_e = \rho u_e$ is calculated by Eqs. (3) and (5), traffic pressure is predicted by Eqs. (7) and (9), with sound speed ratio $c/c_0 = \tau_0/\tau$ obtained by Eq. (10). The dimensionless parameter β is given by

$$\beta = \frac{\nu}{2\tau_0 c_0^2}. \tag{25}$$

The numerical method for Eq. (23) is also TVD (Roe, 1981) as described in Section 3. It is noted that the discretization of $[(2\beta c_0)\cdot(c/c_0)\rho]_x$ is implemented by a second order upwind scheme (Tao, 2001).

4.1. Parameters and conditions

Using the UGM and the extended model (Zhang, 2003), numerical simulations of ring traffic flows are performed for validation. The road length is x_{lmax}=800, with a length unit (i.e. mesh length) l_0 =100 m, a velocity scale $v_0 = q_0/\rho_m \approx$ 2.538 m/s, and time scale $t_0 = l_0/v_0 (\approx 39.414$ s). Other parameters, including free flow speeds v_{fj}, jam density, braking distances $X_{\mathrm{br}j}$ and average length of vehicles l are given in Table 1, and the 1st critical density ρ_{*j} is obtained from Eq. (11). The second critical speed is assumed to be 15 km/h (Zhu and Yang, 2013), which gives $\Lambda_1 = 2.196,\ \Lambda_2 = 2.458,\ \rho_{c21} = 0.6342\rho_m,\ \rho_{c22} = 0.666\rho_m$. When the average vehicle length $l = 5.8$ m, and jam density $\rho_m = 172$ veh/km, as given in Table 1 are used, the dimensionless parameter α has a value 0.9976, for which the dependence of traffic pressure p and sound speed ratio c/c_0 on density ρ are shown in Fig. 3, merely for the case of initial ring road density $\rho_0 = 0.2$.

The blue curve in Fig. 3 indicates that traffic pressure grows with the increase of density monotonically, for $\alpha = 0.9976$, from $p = 0$ on empty road ($\rho = 0$) to $p_m \approx 10$ on completely jammed road ($\rho = 1$). For all free flow states $\rho \le \rho_*,\ \rho_*$ estimated by Eqs. (6) and (11) is equal to 0.1098, traffic pressure p holds a value less then 0.30%; for unsaturated traffic flows $\rho \in (\rho_*,\ \rho_s)$, with the saturation point $\rho_s = 1/e \approx 0.368,\ e$=2.71828, p holds a value in the range (0.3%, 1.38%); for oversaturated traffic flows having a density less than second critical density $\rho_{c2} = 0.655$ [based on Eq. (6)] for braking distances $X_{\mathrm{br}1} = 60$ m and $X_{\mathrm{br}2} = 45$ m, $\rho \in [\rho_s,\ \rho_{c2})$, p is located in the range [1.38%, 4.49%). It can be seen that the traffic pressure grows more rapidly when traffic density is beyond its second critical value. The pressure approaches a value of about 10 for the case of $\rho = 1$.

The black curve in Fig. 3 indicates that traffic sound speed ratio c/c_0 also grows with the increase of density monotonically. Even for the case when the road is empty, i.e. $\rho = 0$, the sound speed ratio has a value of 0.344. On the other hand, when traffic flow is completely jammed, it is approximately equal to 143.2. In particular, at traffic saturation point ρ_s, $c/c_0 = 0.543$.

Initial density condition is assumed to be

$$\rho(0, x) = \begin{cases} 1, & \text{for } x = \in [x_I - 1/2, x_I + 1/2], \\ \rho_0, & \text{Otherwise,} \end{cases} \tag{26}$$

$$\rho_1(0, x) = \begin{cases} 1/3, & \text{for } x \in [x_I - 1/2, x_I + 1/2], \\ 0.05, & \text{Otherwise,} \end{cases} \tag{27}$$

with $q(0, x) = q_e(\rho(0, x))$. As shown in Fig. 3, x_I $(I = A, B, C, D)$ is calculated from values given in Table 1, with Reynolds number (Re $= l_0 v_0/\nu$) of 32, and $2\beta = 7.7425 \times 10^{-3}$. The viscoelasticity parameter denoted by $\gamma = \left[\frac{2G(\tau_0 v_0)}{l_0^2} \cdot \frac{t_0}{q_0}\right]$, has a value of 0.03125 (Smirnova et al., 2017). The model validation is based on the comparison of numerical simulations of ring traffic flows for three cases of ρ_0=0.2, 0.368 and 0.5, with the values of ramp flow parameters $\sigma_{1\mathrm{av}}$ and $\sigma_{2\mathrm{av}}$ having values as given by Table 1.

In addition to the artificially assumed four initial jams located at x_I $(I = A, B, C, D)$, we have assumed on the ring road, initial urgent density fraction should be $s_0 = 0.05/\rho_0$, which is different from the s_0 value (1/3) at x_I. This difference allows to explore the impacts of urgent driving behavior on traffic flow characteristics and travel time on the ring road.

4.2. Comparison of results

Traffic flow patterns in the $t - x$ plane given by density contours are shown in Fig. 5(a–c), where left part shows the flow patterns based on the EZM, while right part shows the patterns based on the present UGM. The density in the blue region is less than 0.2, while in the red region it is higher than 0.7, with the other colored regions having values given by the figure legend. From Fig. 5(a–c), it is seen that the on and off ramp flows have significant influences on the traffic patterns in the $t - x$ plane, the patterns depend on the initial density ρ_0 on the ring road. In particular, from Fig. 5(b), it can be seen the on ramp flow can cause traffic jams spreading backward, accompanying with the jams propagation and the interaction of rarefaction waves, congested traffic pattern upstream the on ramp intersection X_{R2} (schematically shown in Fig. 2) can be observed. The similarity of traffic wave structure to that obtained by the EZM, to some extent indicates that the UGM is reasonable.

Temporal evolutions of traffic density and acceleration at $x = 400$ for ρ_0=0.2, 0.368, and 0.5 are shown in Fig. 6(a–c), where R/ρ has been measured by 1.5 m/s^2 (the permitted maximum acceleration). Correspondingly, a negative drop of acceleration (R/ρ) accompanies with a positive peak of density (ρ). At $x = 400$, the evolutional waves of ρ and R/ρ have different shapes. However, discrepancies between the evolution curves do not justify model reliability, as the absolute value of traffic flow acceleration in the time period $t \in (0, 5\,\mathrm{h})$ is generally less than unity.

Evolutions of urgent density fraction at $x = 400$ for the three initial values of ρ_0 are given by Fig. 7(a–c). As mentioned in Section 4.1, the initial urgent fraction is certainly estimated by $s_0 = 0.05/\rho_0$. Since at the initially assumed jams the urgent density fraction is kept at 1/3, the traffic jam propagation and interaction with deflation waves, under the influences from the ramp flows, at the fixed section $x = 400$, the instantaneous variation of s shown by solid green line calculated by the UGM is similar to that shown by dashed black line obtained by the EZM. The variation of s is less similar to the variation of traffic density, but strongly depends on initial density ρ_0. The larger the initial density ρ_0, the less is the peak number of the evolution curve. Similar to those evolution curves given by Fig. 6(a–c), the evolutions of s at the three values of ρ_0 are consistent with the spatial-temporal traffic flow patterns in Fig. 5(a–c).

The comparison indicates that numerical results based on the UGM are reliable, with the spatial-temporal evolutions reflecting the structure of traffic shock waves in the $t - x$ plane. The numerical results provide a data base to estimate travel time on the ring road with ramp effects when local average speed can be obtained by averaging traffic speed in a pre-assigned time period Δ_0.

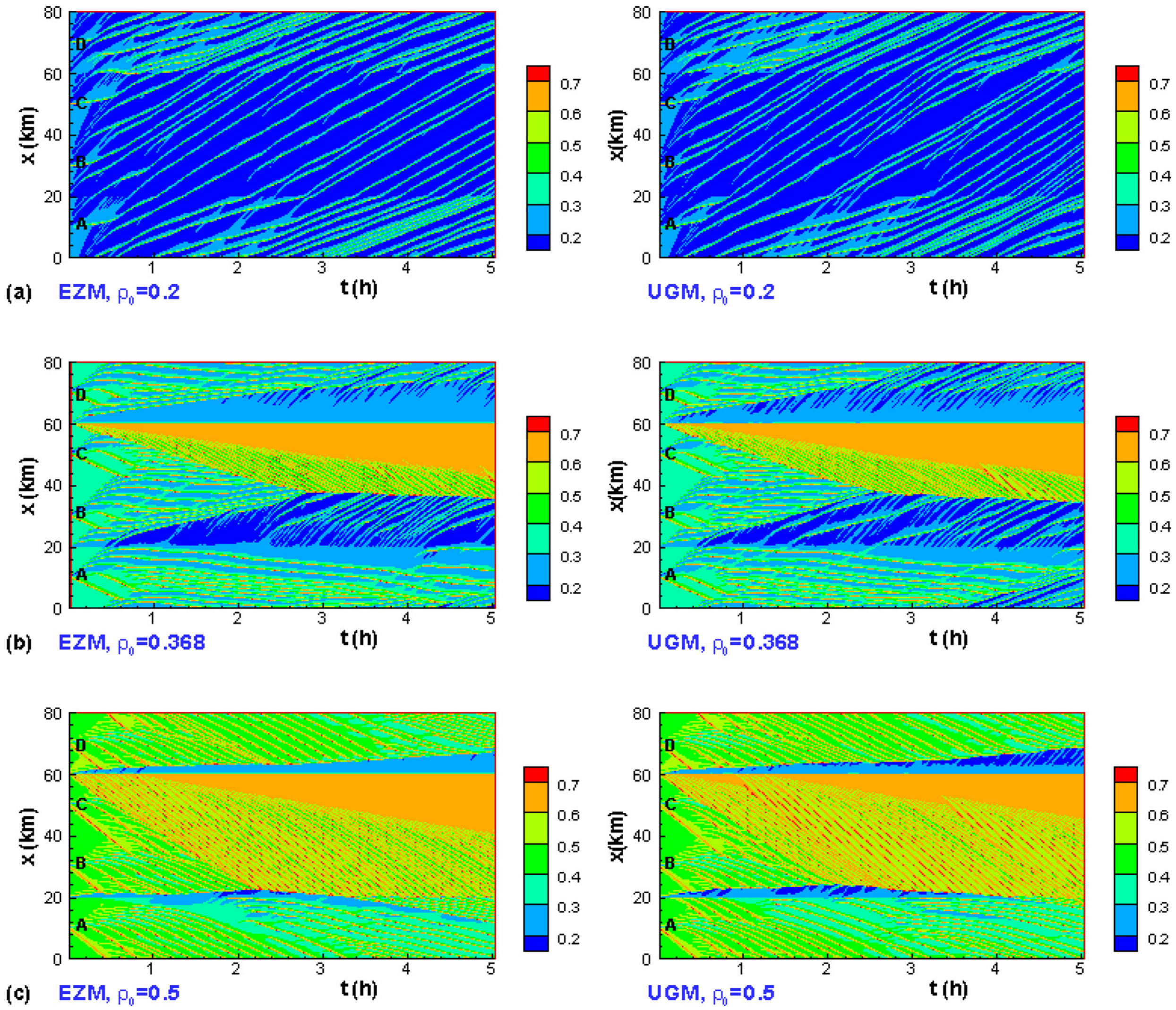

Fig. 5. Spatial-temporal evolutions of traffic density on the ring road, (a) $\rho_0 = 0.2$; (b) for $\rho_0 = 0.368$; (c) for $\rho_0 = 0.5$.

5. Results and discussion

5.1. Simulation parameters

Using the EZM and the present UGM, with the traffic fundamental diagram shown in Fig. 1, numerical tests of traffic flows on ring road as schematically shown in Fig. 2, are carried out to estimate traffic density dependence of average travel time T_{tav} and its root mean square value T_{t}'. The ring road has a total length $L = 80$ km, while the initial ring traffic has a free flow speed based on $v_{f1} = 100$ km/h (urgent), $v_{f2} = 80$ km/h (gentle), and initial urgent density fraction $s_0(x) = \rho_1(0, x)/\rho(0, x)$, with other traffic flow parameters given in Table 1.

Traffic jam density 172 veh/km, is exactly identical to the integer of $1000/l$, with l denoting average vehicle length 5.8 m. The free flow speed for gentle class v_{f2} is set as 80 km/h, the braking distance X_{br2} is taken as about 45 m, as selected for a VAZ type vehicle (Kiselev et al., 2000). While the free flow speed for urgent class v_{f1} is set as 100 km/h, the braking distance X_{br1} is taken as 60 m, as a result of discussion with some drivers around. It is assumed that traffic length scale l_0 is equal to 100 m, corresponding to the relaxation time $\tau_{01} (= l_0/c_{\tau 1} \approx 8.082$ s) and $\tau_{02} (= l_0/c_{\tau 2} \approx 9.765$ s). The visco-elasticity in the UGM $\gamma [= \frac{2G(\tau_0 v_0)}{l_0^2} \cdot \frac{t_0}{q_0}]$ is assumed as 0.03125, relevant to a 2β value of 7.7425×10^{-3} in the EZM.

The initial density is assigned with Eqs. (26) and (27). The initial jams are strictly assumed to be positioned at four grid points X_I, $(I = A,\ B,\ C,\ D)$ [see, in Fig. 2]. The behavior of these jams' propagation is extremely dependent on the value of ρ_0 and ramp flows, in addition to the sensitive influences from the visco-elasticity γ as reported recently (Smirnova et al., 2017).

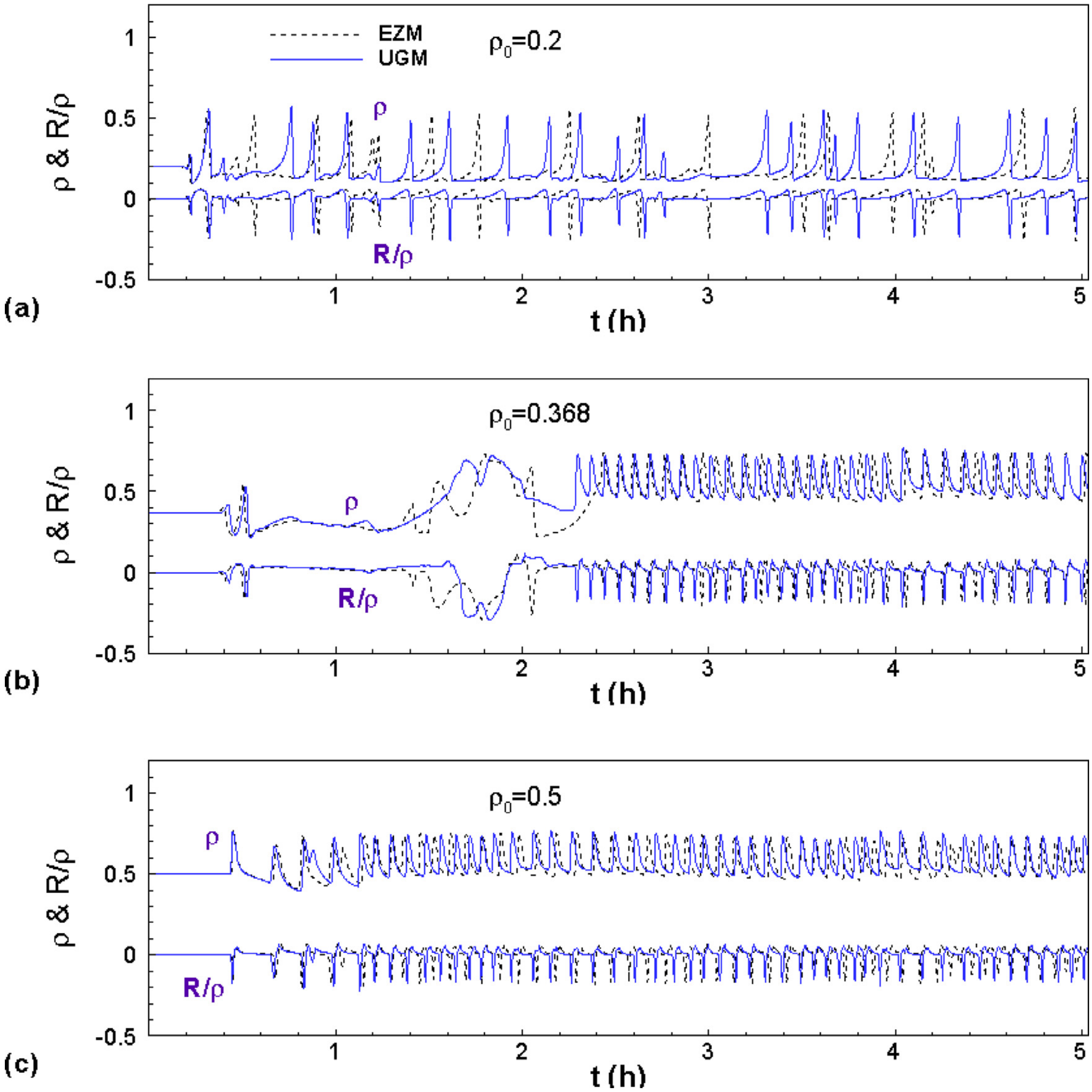

Fig. 6. Temporal evolutions of traffic speed and density at x=40km for (a) ρ_0=0.2; (b) ρ_0=0.368; (c) ρ_0=0.5.

The travel time T_t on the ring road is calculated with the local average speed $\overline{u}_k(t)$ based on a pre-assigned time period Δ_0 and the road length L. When the total space grid number is $N = 801$, we have $L = (N-1) * l_0$, indicating it equals 80km exactly. Hence, if we introduce Δ_0, the instantaneous travel time $T_t(t)$ is written as

$$T_t(t) = \sum_{k=1}^{N-1} l_0/\overline{u}_k(t), \tag{28}$$

where

$$\overline{u}_k(t) = \frac{1}{\Delta_0}\int_{t-\Delta_0}^{t} u_k(\xi)d\xi,$$

with Δ_0=7.5 min.

Since traffic jams propagation results in traffic speed and density have evident time dependent properties, we have to predict the travel time by means of time averaging for $T_t(t)$, which also allows one to calculate the relevant root means square of travel time. Hence, we have the mean travel time

$$T_{tav} = \frac{1}{t_{end} - t_0}\int_{t_0}^{t_{end}} T_t(\xi)d\xi, \tag{29}$$

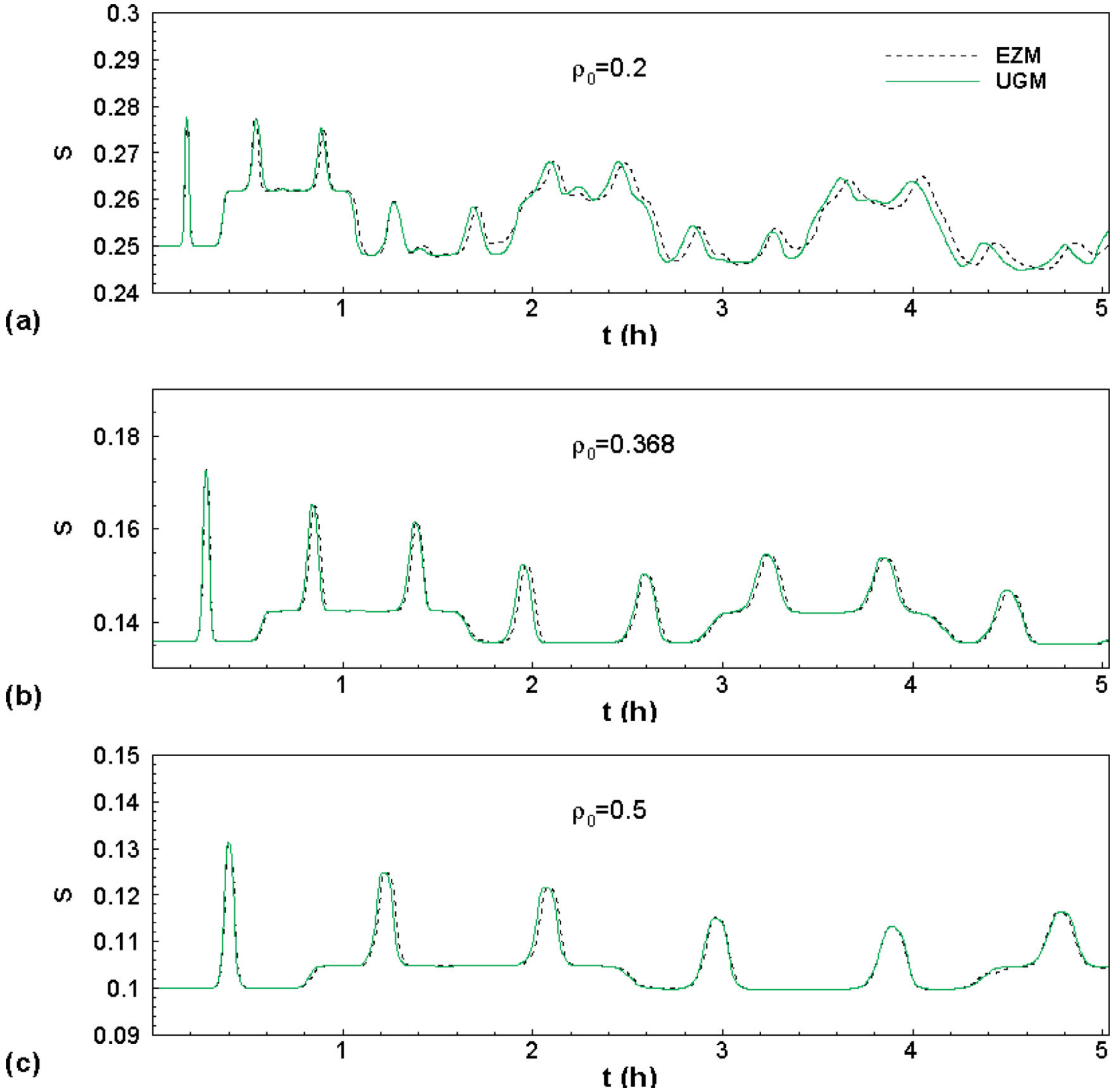

Fig. 7. Temporal evolutions of urgent density fraction s at x =40km for (a) ρ_0=0.2; (b) ρ_0=0.368; (c) ρ_0=0.5.

with the root means square T_t' satisfying

$$[T_t']^2 = \frac{1}{t_{\text{end}} - t_0} \int_{t_0}^{t_{\text{end}}} [T_t(\xi) - T_{\text{tav}}]^2 d\xi, \tag{30}$$

here t_0 represents initial time, in general $t_0 = 0$, with t_{end} denoting the time of terminating the numerical simulation.

It is necessary to explain that traffic pressure p and traffic sound speed c so far have not gotten unified modeling. In gas-kinetic model (Helbing and Treiber, 1998; Hoogendoorn and Bovy, 2000), p is considered to be dependent on the traffic speed fluctuation; while in Navier–Stokes like model (Kerner and Konhäuser, 1993; Zhang, 2003; Zhu and Yang, 2013), p is taken as a function of traffic density. Sound speed c has been linked to the derivative of equilibrium speed with respect to density (Payne, 1971; Zhang, 2003), related to the braking distance to vehicles X_{br}, and derived from the definition of classical mechanics (Bogdanova et al., 2015; Smirnova et al., 2017). In viscoelastic modeling of traffic flow, the point of view suggesting p be proportional to the reciprocal of space headway, certainly has its own reason-ability, as the headway closes to zero, traffic pressure approaches to infinity, giving a strong demand of stoppage.

Therefore, in the present numerical simulations of ring traffic flows based on the UGM and EZM, for the convenience of comparison, a remedy is given mainly in describing sound speed, pressure, and urgent density fraction. In the numerical tests, it is also assumed the product $[c\cdot\tau]$ is a constant. Fig. 3 shows traffic pressure (a) and traffic sound speed ratio c/c_0 (b) just for $\rho_0 = 0.2$, where c_0 is the traffic sound speed at second critical density ρ_{c2}. Both curves are slightly dependent on the initial urgent density fraction.

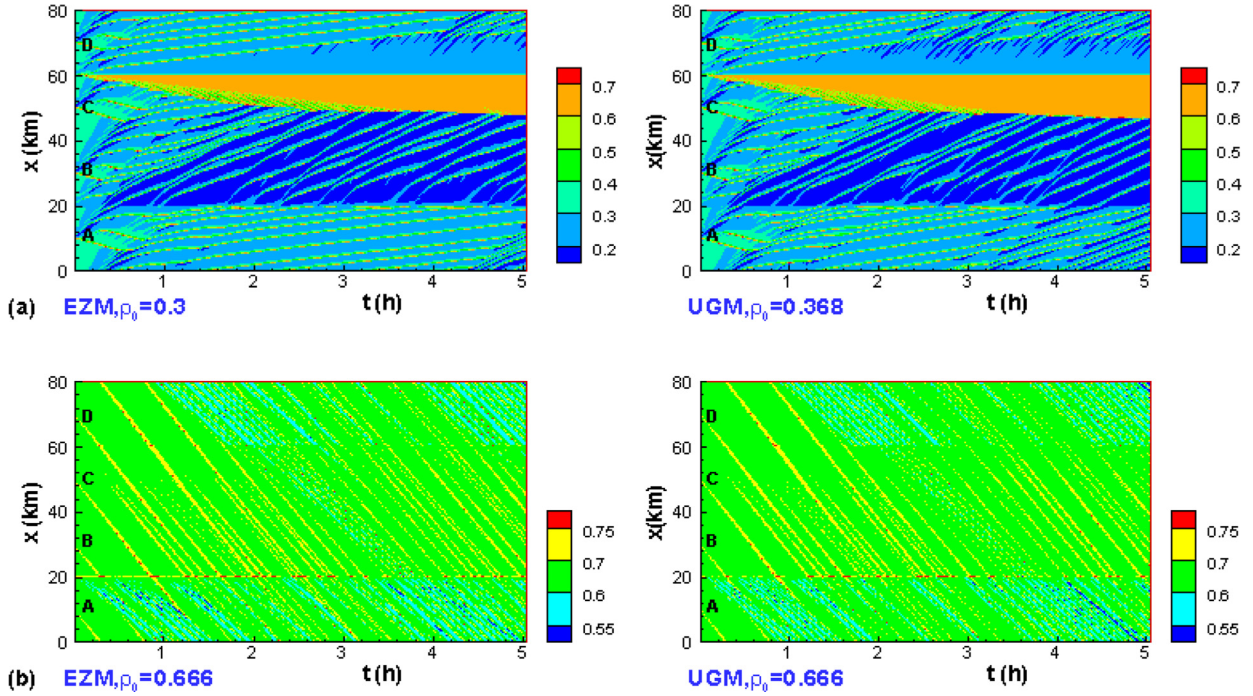

Fig. 8. Spatial-temporal evolutions of traffic density on the ring road without ramp-effect, (a) $X_{br1} = 45$ m; (b) $X_{br1} = 60$ m.

Sound speed plays a significant role of interaction between traffic waves, as it in fact examines two slopes of characteristic lines, implying traffic pressure is a crucial parameter in mathematical modeling of traffic flow, which has impacts on the propagation and structure as well as the spontaneous generation of traffic shock waves. To date, quantitative description of traffic pressure has less been reported.

5.2. Traffic flow patterns

To seek the effect caused merely by urgent class, the flow patterns obtained without ramp effect are shown in Fig. 8(a and b), where part (a) illustrates the spatial-temporal evolution of ring road density when the so-call urgent class is false, as the braking distance and free flow speed of urgent class are equal to that of the gentle class, labeled by $X_{br1} = 45$ m, and part (b) shows the relevant evolution of ring road density in the case of $X_{br1} = 60$ m. The comparison between part (a) and (b) indicates that there do have some differences in flow patterns, but merely slight, implying that the effect of urgent driving behavior on travel time should be small.

It is noted for $X_{br1} = 80$, the free flow speed is selected to be 120 km/h, with 1st and 2nd critical density equal to 0.0676 and 0.6034. To show the effect caused by the braking distance of urgent class, Fig. 9(a–c) show the flow patterns with ramp effect (σ_{1av} and σ_{2av} seen in Table 1) by spatial-temporal evolutions of ring road traffic speed at three values of initial density ρ_0, and two values of braking distance X_{br1}.

In Fig. 9(a), for the case of $\rho_0 = 0.2$, the initially assumed traffic jams propagate forward. The off ramp flow located at intersection X_{R1} in general increases the traffic flow speed in the road segment $x \in (X_{R1}, X_{R2})$. A comparison between the left and right part reveals that the change of X_{br1} does have brought about some variation of traffic flow patterns.

In Fig. 9(b and c), it is seen that the larger the braking distance X_{br1}, the larger is the congested flow region upstream the on-ramp intersection X_{R2}. It is seen that an increase of X_{br1} has enlarged the backward propagation shock intensity originated at the on-ramp intersection. The initial jams cause spontaneously generated jams between them. These spontaneously generated jams are similar to those narrow jams found in the data measured on German highways (Kerner, 1998), they start to move backward, but due to interaction with traffic rarefaction waves and ramp flows, similar to the initial jams, the spontaneous jams change intensity, and structure and propagation direction.

It is found that traffic flow patterns on the ring road are extremely dependent on initial density ρ_0, which denotes the spatially averaged density on the ring road. The propagation speeds of jams are closely dependent on the wave interaction and the fundamental diagram used in the numerical test, as explained by Daganzo (1997) and recent works (Lebacque et al., 2007; Zhang et al., 2009; Lebacque and Khoshyaran, 2013; Smirnova et al., 2017).

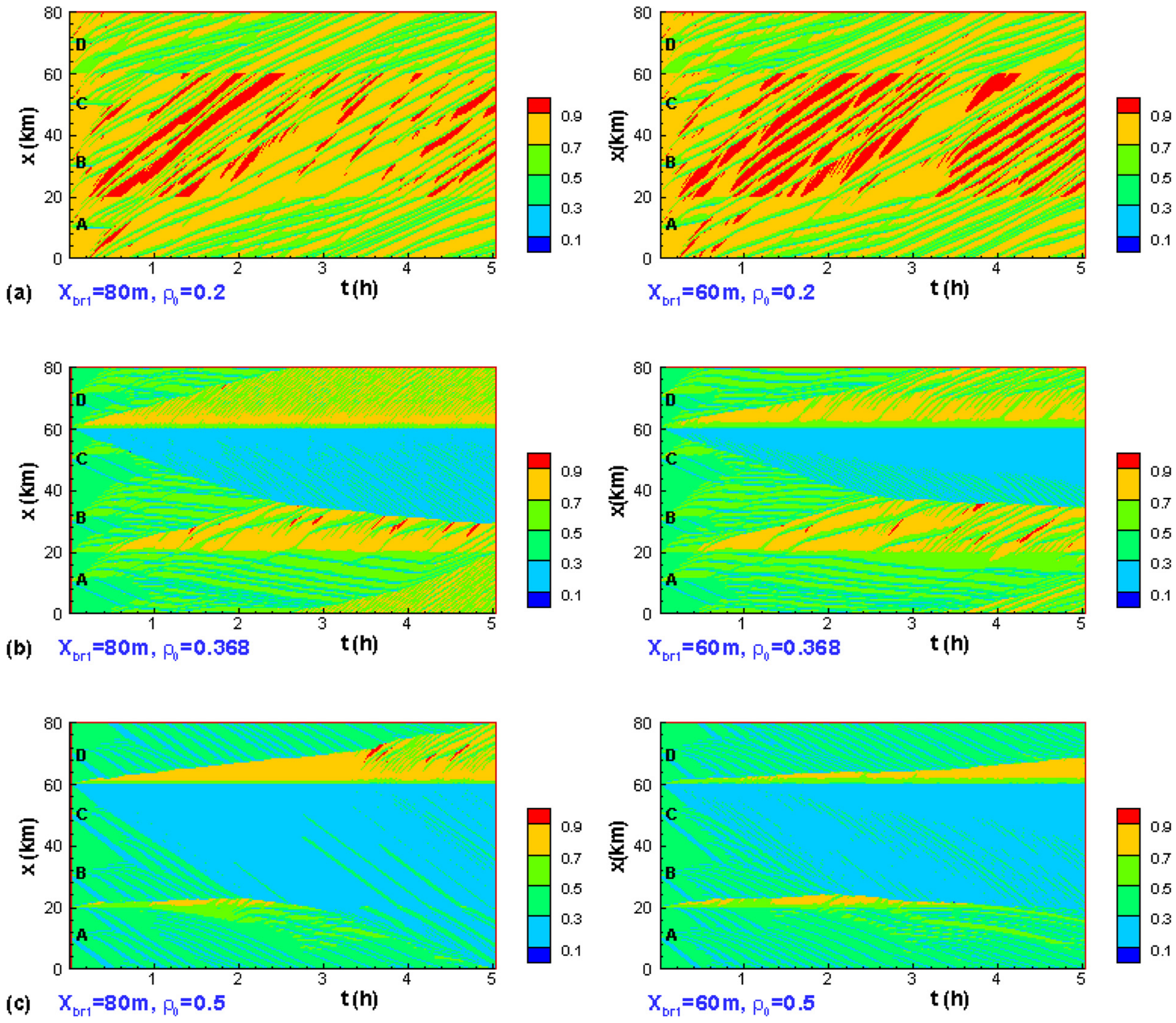

Fig. 9. Spatial-temporal evolutions of traffic speed on the ring road at different braking distance X_{br1}, (a) ρ_0=0.2; (b) ρ_0=0.368, (c) ρ_0=0.5. Note that the evolutions are obtained by the UGM.

5.3. Evolutions of density and speed

Temporal evolutions of traffic flow speed and density at $x = 400$ are shown in Fig. 10(a–d) for four values of ρ_0. When the density ρ_0=0.2, which is less than the saturation density $\rho_s(= 0.368)$ but beyond 1st critical density ρ_*, as shown in Fig. 10(a), on the ring road, the commonly observed traffic flow mode is stop-and-go type, as the speed evolution curve oscillates like stop and moving waves (Kühne and Michalopoulos, 2001; Castillo, 2001). The oscillation of speed has one to one correspondence with that of traffic density, i.e., a valley of speed corresponds to a positive pulse of density.

As shown in Fig. 10(b), when the initial density ρ_0 is equal to the saturation density ρ_s, there exist oscillations accompanied by several peaks and negative pulses on the evolution curves of density and speed, as a results of traffic jams propagation and traffic waves interactions. The speed oscillations at $x = 400$ reflects the nonlinearity of the governing equation of traffic speed, implying the estimated travel time on the rind road on the basis of traffic models may have uncertainty to a certain extent.

Being consistent with the right traffic pattern in Fig. 5(c), the evolutions of density and speed at $x = 400$ for initial density $\rho_0 = 0.5$ are shown in Fig. 10(c). For the over saturated traffic flow, the initial jams propagate backward, the on ramp flow has generate a large amount of jams spreading backward, the prevailing traffic flow mode is stop-and-go type. Observing together with the right traffic pattern in Fig. 5(c), it is seen that the 1st left pulse of density is relevant to the initially assumed jam at X_C, with the 2nd, 3rd, and 4th left pulses of density corresponding to the three spontaneously generated jams (Kerner, 1998).

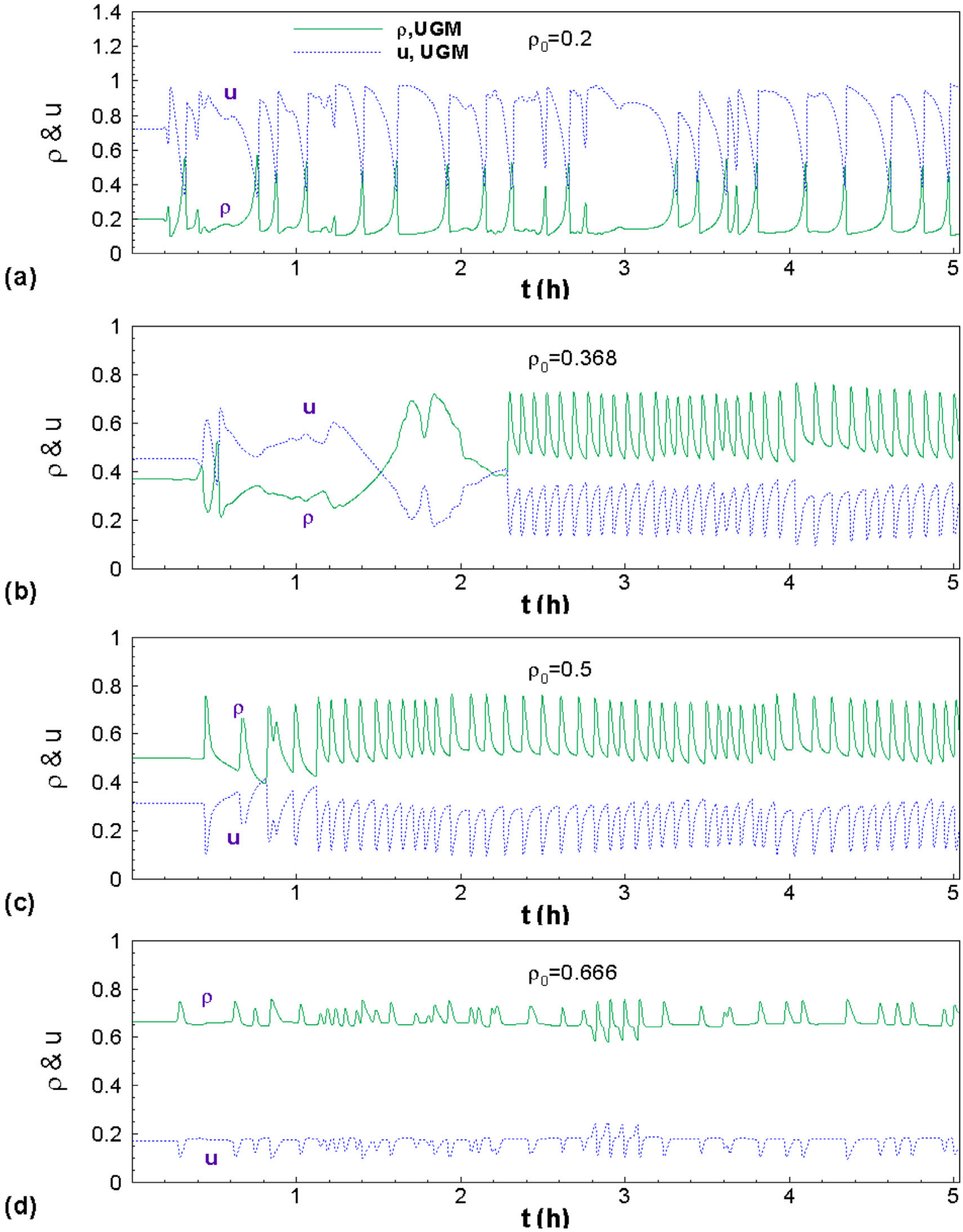

Fig. 10. Evolution of ρ and u at section $x = 40$ km for (a) $\rho_0 = 0.2$; (b) $\rho_0 = 0.368$; (c) $\rho_0 = 0.5$, and (d) $\rho_0 = 0.666$.

In Fig. 10(d), the evolution curves of density and speed at $x = 400$ for initial density $\rho_0 = 0.666$ are illustrated. As the initial density is identical to 2nd critical density of gentle class ρ_{c22}, at which the equilibrium speed is 0.1875 in the unit of v_{f2}. As the on ramp flow flux is approximately equal to the off ramp flow flux, mainly controlled by random number σ_1 and q, at $x = 400$, the traffic flow speed is oscillating around the equilibrium speed, with the speed evolution depending on traffic jams propagation and interaction.

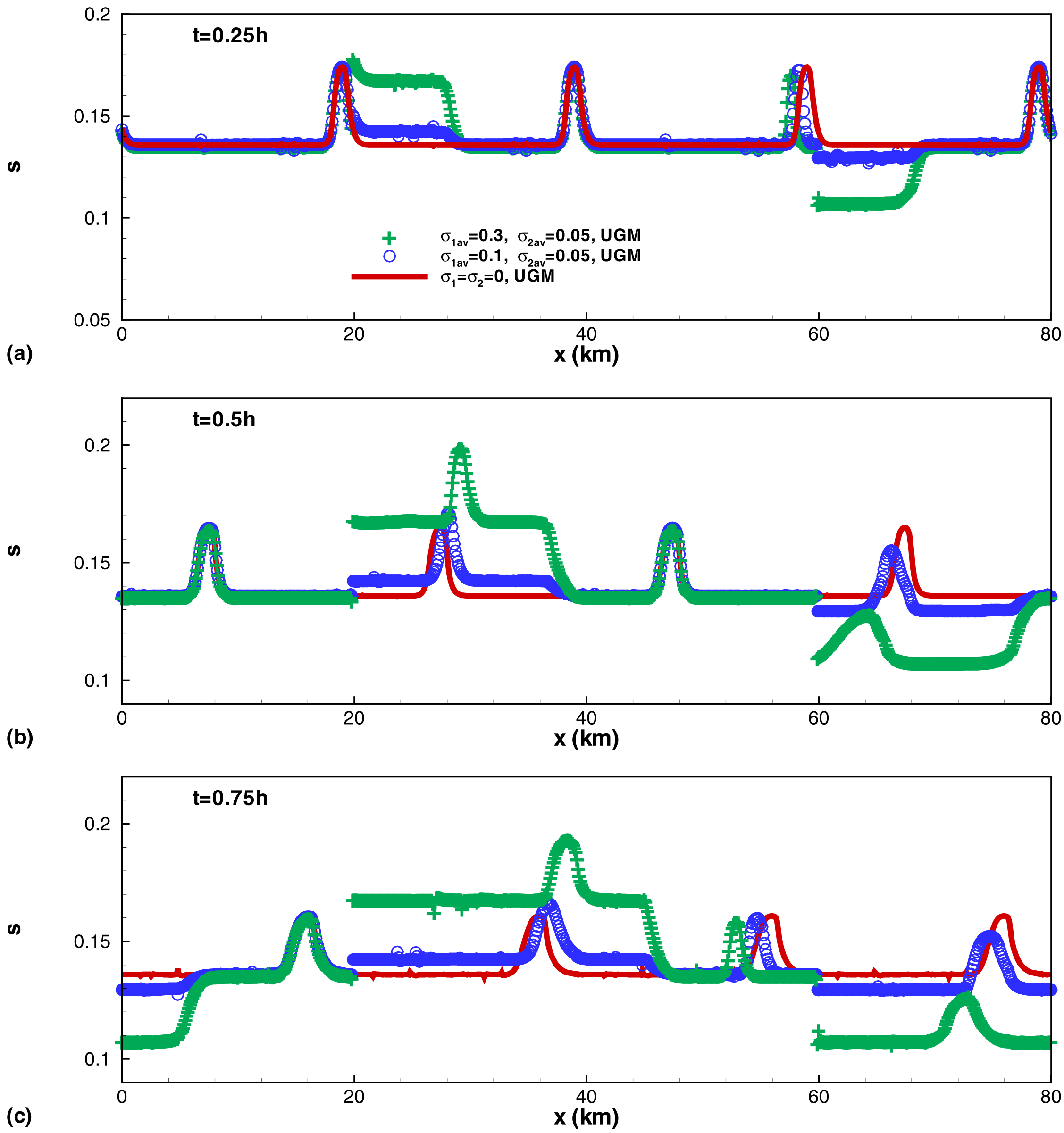

Fig. 11. Distribution of urgent density fraction s on the ring road in the case of $\rho_0 = 0.368$ at $t = 0.25$h (a), and 0.5h (b).

5.4. Distribution of urgent density fraction

For the saturation case $\rho_0 = \rho_s = 0.368$, the instantaneous distributions of urgent density fraction s on the ring road for three ramp flow cases at $t = 0.25,\ 0.5$, and 0.75 h are shown in Fig. 11(a–c). Since the urgent mass fraction satisfies

$$\frac{\partial s}{\partial t} + u\frac{\partial s}{\partial x} = s(\sigma_2 - \sigma_1)q,$$

the propagation speed of any infinitesimal disturbance of s should be local traffic speed, but not $\partial q/\partial \rho$, indicating that urgent mass fraction s should have different evolution behaviors from that of traffic density ρ.

In Fig. 11(a), without ramp effect, i.e. $\sigma_1 = \sigma_2 = 0$, the solid red line shows that the four s peaks at the time of $t = 0.25$ h is located at x=19, 39, 59 and 79 km. It means that the initially assumed s peaks with a value of 1/3 at x_I $(I = A, B, C, D)$ have propagated forward with average speed of about 36km/h, a value rather close to the equilibrium speed $u_e(\rho_s)(= 0.454)$ in the unit of v_{f2}. As ramp flow can bring about significant changes of traffic flow pattern, naturally resulting in large traffic speed variation on the main road, such a ramp effect can also be seen from the distribution curves of urgent density fraction s. From Fig. 11(a), it is seen that some deviations of blue circles and green plus '+' symbols around the ramp intersections

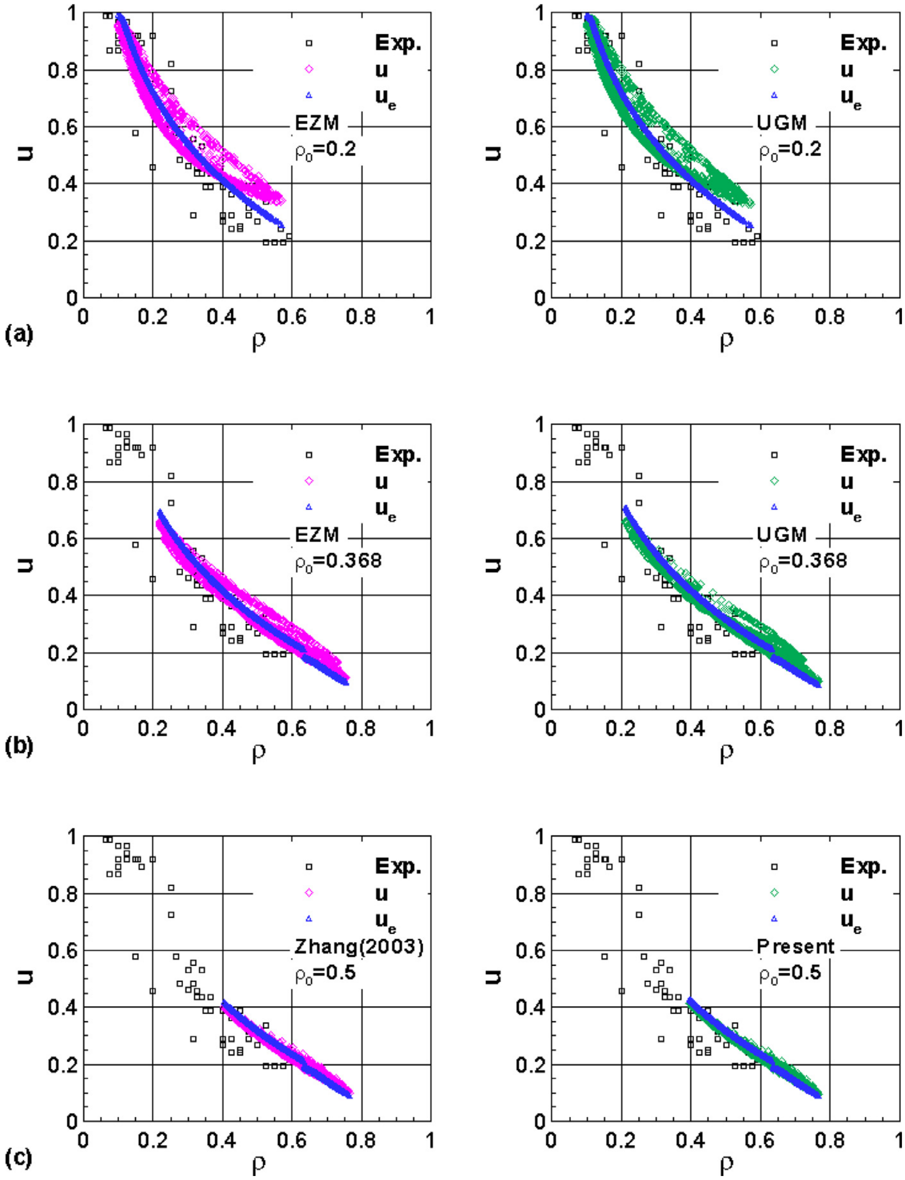

Fig. 12. Comparison of traffic speed with existing measured data at $x = 40$ km for (a) ρ_0=0.2; (b) ρ_0=0.368, (c) ρ_0=0.5. The observation data are obtained from McShane et al. (1998), and the jam density for normalisation is supposed to be 200 veh/mile.

X_{R1} (= 20 km) and X_{R2} (= 60 km) certainly exist, the deviations from the solid red line becomes larger with the increase of ramp parameter σ_{1av}.

The ramp effect plus traffic wave interactions and propagations on the main road, can lead to more apparent deviations of $s-$ curves from the solid red curve corresponding to the situation without ramp effect, as seen in Fig. 11(b–c). At the time of $t = 0.5$h, from Fig. 11(b), it is seen that the off-ramp flow caused speed variation, results in the occurrence of the blue peak at $x = 28.01$km and the green peak at x=29.2km at the right side of the red one at $x = 27.7$ km, while the speed variation caused by on-ramp flow leads to the blue and green peaks respectively at $x = 64.4$ and 66.25 km appear at the left side of the red peak at $x = 67.7$ km. The off-ramp flow and on-ramp flow can respectively induce a decrease and an increase of urgent density fraction s in the relevant segment downstream the ramp intersection. The length of the ramp flow impacted segment increases with time, as can be seen in Fig. 11(c).

5.5. Comparison with measured data

In Fig. 12(a–c), the instantaneous traffic speed (u) at $x = 40$ km is illustrated as a function of traffic density for three values of initial density $\rho_0 = 0.2$ 0.368, and 0.5, together with the relevant instantaneous equilibrium speed

Table 2
Density dependence of T_{tav} and T_t' for $\sigma_{1av} = 0.1$, and $\sigma_{2av} = 0.05$.

	UGM		EZM			UGM		EZM	
ρ_0	T_{tav}(h)	a[a] T_t'(h)	T_{tav} (h)	aT_t'(h)	ρ_0	T_{tav}(h)	aT_t'(h)	T_{tav} (h)	aT_t'(h)
0.1	1.095	0.325	1.105	0.284	**0.5**	**3.322**	**2.770**	**3.350**	**2.715**
0.2	**1.445**	**0.544**	**1.457**	**0.527**	0.55	3.835	3.891	3.866	4.280
0.3	1.988	4.023	2.057	4.215	0.6	4.534	5.585	4.574	5.913
0.368	**2.431**	**5.764**	**2.455**	**5.899**	0.633	5.136	4.324	5.178	4.336
0.4	2.635	6.024	2.667	6.737	0.666	5.878	3.388	5.929	3.335
0.45	2.955	5.115	2.986	5.388					

[a] Here a=100, used as a factor merely for the convenience of illustration.

(u_e) at $x = 40$ km determined by Eqs. (3) and (5) as labeled by unfilled blue-triangles, and the measured data of McShane et al. (1998) as labeled by unfilled black squares.

For $\rho_0 = 0.2$, which is between the first critical and saturation points, in Fig. 12(a), relevant to temporal revolutions in Fig. 10(a), the left part is predicted by the EZM, as a result of initially assumed jams propagation, the speed predicted at $x = 40$ km can hold values in the range $u \in [0.3352, 0.9712]$, the equilibrium speed has values in an active density range $\rho \in [0.0996, 0.5710]$. The right part is predicted by the present UGM, the speed ranges from 0.328 to 0.981, with the active density range $\rho \in [0.1004, 0.5731]$. The so-called ′active′ refers to that beyond the density range, for the particular case there is no corresponding values for u and u_e. The measured data is scattered, the predicted equilibrium speed (u_e) curve formed by unfilled blue triangles can pass through the data points, with the instantaneous speed u labeled by unfilled green circles falling on the two sides of the u_e curve. It can be seen that the predicted speed at unsaturated situations has taken some value completely in the range of measured data, but for those saturated traffic states relevant to $\rho \geq \rho_s$, the predicted speed is usually over the equilibrium speed u_e. The primary reason is that initial ring traffic is under-saturated, as shown in Fig. 5(a), hence the average speed of spreading of stop-and go wave on ring road is faster, from a traffic jam whether it is initially originated or spontaneously generated, vehicles usually have a faster escaping speed than the equilibrium speed in locally over-saturated scenarios.

As shown in Fig. 12(b), for $\rho_0 = \rho_s$, there exist density and speed oscillations caused by interaction and propagation of traffic waves and ramp flow effect. Consistent with the solid and dashed curves for density and speed evolutions at saturation point as shown in Fig. 10(b), Fig. 12(b) shows these dependencies of u and u_e on traffic density. Note that for $\rho_0 = \rho_s$, $x = 40$ km, using the EZM, the equilibrium speed u_e takes a value in an active density range $\rho \in [0.2178, 0.7537]$, which should be $\rho \in [0.2124, 0.7673]$ by the present traffic model. The equilibrium speed is calculated by Eqs. (3) and (5). The predicted dependencies on density usually agrees well with the measured data.

When $\rho_0 = 0.5$, the vehicle aggregation makes initial jams propagate backward, while the role played by rarefaction wave causes a density decrease in the region downstream the jams, as can be seen in flow pattern given by Fig. 5(c). In Figs. 12(c), at $x = 40$ km, the EZM obtains an active density range $\rho \in [0.4034, 0.7651]$; Using the present UGM, it becomes $\rho \in [0.3955, 0.7681]$. The dependencies of u and u_e on density are also consistent with measured data.

The comparison of the $(u - \rho)$ dependence with measured data, shows the ring road traffic flows are rather sensitive to initial density ρ_0, revealing that viscoelastic traffic flow modeling by virtue of traffic and sound speed concepts can provide reliable simulation results.

5.6. Travel time

Different from the study done in last century (Chang and Mahmassani, 1988), which examined two heuristic rules proposed for describing urban commuters' predictions of travel time as well as the adjustments of departure time in response to unacceptable arrivals in their daily commute under limited information, here we present the travel time to pass through the ring road predicted by the EZM and the present urgent-gentle class traffic model.

It is noted that the travel time T_t is estimated using time averaged speed $\bar{u}_k(t)$ when the pre-assigned period Δ_0 for time averaging is fixed at 7.5 min. Because a zero local traffic speed at a given grid can bring a singularity in travel time estimation, the use of period Δ_0 can make the travel time be estimated without meeting singular points, which could exist due to the occurrence of traffic jams. It is noted that for the scenarios with ramp effect the average value T_{tav} and its root means square (rms) value T_t' by Eqs. (29) and (30) are given by Table 2.

5.6.1. Evolution of travel time

For the situations without ramp effect, to seek the response of braking distance of urgent class, the evolution of travel time by Eq. (28) for the cases of $\rho_0 = 0.2$, ρ_s, and 0.5 is shown in Fig. 13. It is seen that when the urgent braking distance is increased from 45 m to 60 m, the travel time is slightly enlarged, implying that for the sake of travel time urgent driving behavior should be given up.

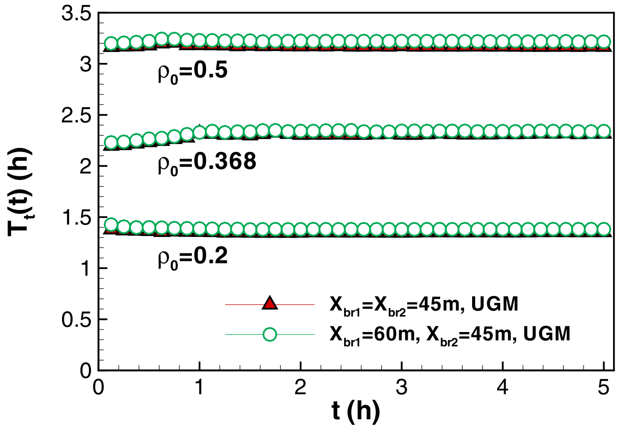

Fig. 13. Travel time T_t versus time on the ring road without ramp effect.

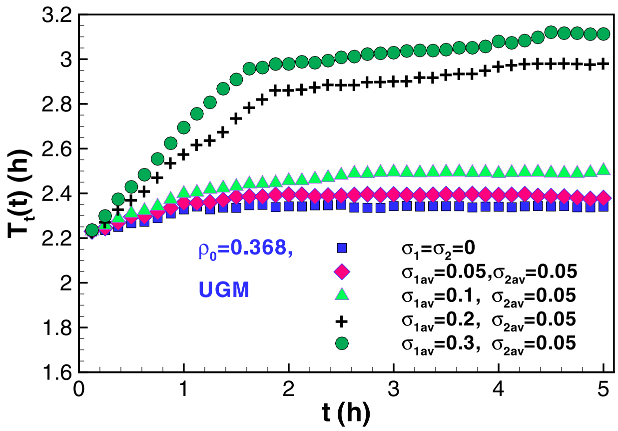

Fig. 14. Travel time T_t versus time on the ring road.

To seek the ramp flow effect, based on the present model, for $\rho_0 = \rho_s$, the evolutions of travel time for different value of ramp parameter $\sigma_{1\mathrm{av}}$ are shown in Fig. 14. The travel time T_{t} on the ring road increase with time, with the increase rate significantly depending on the $\sigma_{1\mathrm{av}}$ value. This reflects that ramp flow can impact the ring road traffic flow dramatically.

5.6.2. Mean travel time and its rms value

For fixed values of ramp parameters, i.e., $\sigma_{1\mathrm{av}} = 0.1$, and $\sigma_{2\mathrm{av}} = 0.05$, the evolution curves of T_{t} for various values of initial density are given by Fig. 15. It is seen that the time variation is related to the initial density, for $\rho_0 = 0.666$, as shown by the green filled circles, the travel time T_{t} decreases with time.

The dependencies of travel time T_{tav} and its root means square (rms) value T_{t}' are shown in Fig. 16(a and b), with the relevant values given by Table 2. It is seen that when the prevailing traffic mode is free flow, such as $\rho_0 = 0.1$, for free flow speed $v_f = 80$ km/h, and ring road length $L = 80$ km, the travel time is about 1.1 h, the negligible delay time 0.1 h is caused by the four initial jams put in $X_I (I = A, B, C, D)$.

For $\rho_0 = 0.2$, the flow patterns given by density and speed contours in the $t - x$ plane are shown in Fig. 5(a) and the right part of Fig. 9(a). The travel time T_{tav} and its rms value are given in Table 2 by bold numbers, indicating that the present UGM has estimated the travel time very close to that calculated by the EZM.

When the initial density ρ_0 is exactly identical to saturation density ρ_s at which the equilibrium speed is $u_{e,s} = 0.454 v_{f2}$, as are given in Table 2 by bold numbers, the travel time T_{tav} is 2.431 h, 2.455 h, calculated respectively by the present UGM and the EZM, corresponding to the two rms values $T_{\mathrm{t}}' = 5.764 \times 10^{-2}$h, 5.899×10^{-2}h.

For $\rho_0 = 0.5$, as given in Table 2 by bold numbers, our numerical tests have estimated two travel time values, the first 3.322 h based on the present model, and the second 3.350 h based on the EZM, corresponding to the two rms values $T_{\mathrm{t}}' = 2.770 \times 10^{-2}$ h, 2.715×10^{-2} h. The mean travel time T_{tav} and its rms value T_{t}' are examined by the traffic flow pattern, as seen in Fig. 5(c).

In general, the mean travel time T_{tav} enhances monotonically with the increase of initial ring road density ρ_0.

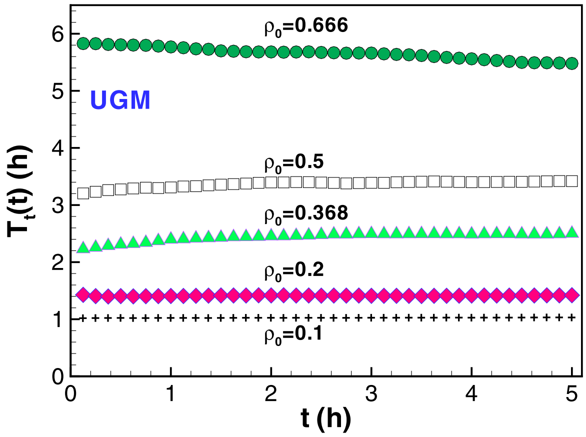

Fig. 15. Travel time T_t versus time on the ring road for ρ_0 =0.1, 0.2, 0.368, 0.5, and 0.666 with ramp effect in the case of $\sigma_{1av} = 0.1$, $\sigma_{2av} = 0.05$.

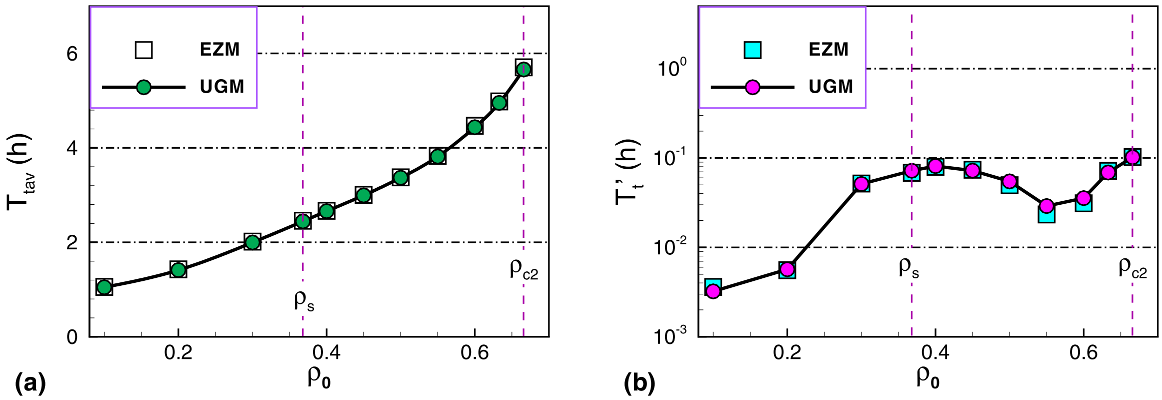

Fig. 16. Dependence of travel time T_{tav} and its rms value T_t' on traffic density on the ring road with total length 80 km with ramp effect in the case of $\sigma_{1av} = 0.1$, $\sigma_{2av} = 0.05$.

6. Conclusions

Traffic pressure plays a crucial role in mathematical modeling of traffic flows. In the present urgent-gentle class traffic flow model, an expression of traffic pressure is derived by postulating that it is proportional to the reciprocal of space headway. Traffic sound speed is rigorously derived from the definition in classical mechanics. Measured by the sound speed defined at the second critical point by braking distance and free flow speed, the sound speed curve has also been illustrated.

Based on descriptions for traffic pressure and sound speed, dividing vehicles into urgent and gentle classes and including viscoelastic and ramp flow effects, we have presented an urgent-gentle class traffic flow model (UGM), which is similar to the extended Navier–Stokes like model developed by Zhang (2003, named EZM). To explore the application potential of the present model, the travel time through a ring road with total length 80 km has been estimated numerically and compared with that using the EZM. An excellent agreement is obtained.

Numerical results reveal that without ramp flow effect, the increase of urgent braking distance can slight change the traffic flow pattern shown by spatial-temporal evolutions. Therefore the urgent driving behavior can slightly change the mean travel time on the ring road, not shorten but delayed a little bit, suggesting that rational management of road operation is necessary.

With ramp effect, the mean travel time predicted by the present model is almost the same as that predicted by the EZM. Each initial jam is assumed to be limited in single grid point, but the assumed four initial jams play significant roles in the formation and evolution of traffic flow patterns. The travel time is mainly dependent on the initial traffic density.

For the free flow speed of gentle class 80 km/h, with the free flow speed of urgent class 100 km/h, when the initial density is slightly lower than the first critical density, the travel time is about 1.1 h; when the ring road has a saturation density, the travel time is around 2.45 h; for the case with initial density equal to the 2nd critical density of gentle class, the travel time is about 5.9 h. The mean travel time T_{tav} enhances monotonically with the increase of initial ring road density.

Acknowledgments

Here we acknowledge the support of Russian Foundation for Basic Research (RFBR Grant 18-07-00518) and NSFC (10972212).

References

Aw, A., Rascle, M., 2000. Resurrection of *second order* models of traffic flow. SIAM J. Appl. Math. 60, 916–938.
Bogdanova, A., Smirnova, M.N., Zhu, Z.J., Smirnov, N.N., 2015. Exploring peculiarities of traffic flows with a viscoelastic model. Transportmetrica A 11(7).
Castillo, J.M.D., 2001. Propagation of perturbations in dense traffic flow: a model and its implications. Transp. Res. Part B 35, 367–389.
Chang, G.L., Mahmassani, H.S., 1988. Travel time prediction and departure time adjustment behavior dynamics in a congested traffic system. Transp. Res. Part B 22(2), 217–232.
Chang, G.L., Zhu, Z.J., 2006. A macroscopic traffic model for highway work zones: formulations and numerical results. J. Adv. Transp. 40(3), 265–287.
Chien, S.I.J., Kuchipudi, C.M., 2003. Dynamic travel time prediction with real-time and historic data. ASCE J. Transp. Eng. 129(6), 608–616.
Chowdhury, D., Santen, L., Schadschneider, A., 2000. Statistical physics of vehicular traffic and some related systems. Phys. Rep. 329, 199–329.
Costeseque, G., Lebacque, J.P., 2014. A variational formulation for higher order macroscopic traffic flow models: numerical investigation. Transp. Res. Part B 70, 112–133.
Daganzo, C.F., 1997. Traffic flow theory. In: Daganzo, C.F. (Ed.), Fundamentals of Transportation and Traffic Operations. Pergamon, New York, pp. 67–160.
Dailey, D.J., 1993. Travel-time estimation using cross-correlation techniques. Transp. Res. Part B 27(2), 97–107.
Hans, E., Chiabaut, N., Leclercq, L., 2015. Applying variational theory to travel time estimation on urban arterials. Transp. Res. Part B 78, 169–181.
Helbing, D., 2001. Traffic and related self-driven many-particle systems. Rev. Mod. Phys. 73, 1067–1141.
Helbing, D., Huberman, B.A., 1998. Coherent moving states in highway traffic. Nature 396 (6713), 738–740.
Helbing, D., Treiber, M., 1998. Gas-kinetic-based traffic model explaining observed hysteretic phase transition. Phys. Rev. Lett. 81, 3042–3045.
Hofleitner, A., Herring, R., Bayen, A., 2012. Arterial travel time forecast with streaming data: a hybrid approach of flow modeling and machine learning. Transp. Res. Part B 46, 1097–1122.
Hoogendoorn, S.P., Bovy, P.H.L., 2000. Continuum modeling of multiclass traffic flow. Transp. Res. Part B 34(2), 123–146.
Jenelius, E., Koutsopoulos, H.N., 2013. Travel time estimation for urban road networks using low frequency probe vehicle data. Transp. Res. Part B 53, 64–81.
Kerner, B.S., Konhäuser, P., 1993. Cluster effect in initially homogemeous traffic flow. Phys. Rev. E 48, 2335–2338.
Kerner, B.S., 1998. Experimental features of self-organization in traffic flow. Phys. Rev. Lett. 81(17), 3797–3800.
Kiselev, A.B., Nikitin, V.F., Smirnov, N.N., Yumashev, M.V., 2000. Irregular traffic flow on a ring road. J. Appl. Math. Mech. 64(4), 627–634.
Kühne, R. D., Michalopoulos, P., 2001. Continuum flow models. http://www-cta.ornl.gov/cta/research/trb/tft.html.
Kumar, B.A., Vanajakshi, L., Subramanian, S.C., 2017. Bus travel time prediction using a time-space discretization approach. Transp. Res. Part C 79, 308–332.
Ladino, A., Kibangou, Y., Canudas de Wit, C., Fourati, H., 2017. Travel time prediction and departure time adjustment behavior dynamics in a congested traffic system. Transp. Res. Part C 80, 216–238.
Lebacque, J.P., Khoshyaran, M.M., 2013. A variational formulation for higher order macroscopic traffic flow models of the gsom family. Transp. Res. Part B 57, 245–265.
Lebacque, J.P., Mammar, S., Haj-Salem, H., 2007. Generic second order traffic flow modelling. In: Allsop, R., Benjiamin, G. (Eds.), Transportation and Traffic Theory. Elsevier, Oxford, pp. 755–776.
Li, J., Zhang, H.M., 2013. The variational formulation of a non-equilibrium traffic flow model: theory and implications. Procedia - Soc. Behav. Sci. 80, 327–340.
Lighthill, M.J., Whitham, G.B., 1955. On kinematic waves ii: a theory of traffic flow on long crowded roads. Proc. Roy. Soc. Lond A 229, 317–345.
Lint, J.V., der Zijpp, N.V., 2003. Improving a travel-time estimation algorithm by using dual loop detectors. Transp. Res. Rec. J. Transp. Res. Board 1855.
Ma, J., Chan, C.K., Ye, Z.B., Zhu, Z.J., 2017. Effects of maximum relaxation in visco-elastic traffic flow modelling. Transp. Res. Part B. Accepted, TRB2003.
Ma, Z.L., Koutsopoulos, H.N., Ferreira, L., Mesbah, M., 2017. Estimation of trip travel time distribution using a generalized markov chain approach. Transp. Res. Part C 74, 1–21.
McShane, W.R., Roess, R.P., Prassas, E.S., 1998. Calibration relationships for freeway analysis. In: McShane, W.R., Roess, R.P., Prassas, E.S. (Eds.), Traffic Engineering. Prentice-Hall, New Jersey, pp. 282–306.
Nagatani, T., 2002. The physics of traffic jams. Rep. Prog. Phys. 65, 1331–1386.
Nagel, K., Schreckenberg, M., 1992. A cellular automaton model for freeway traffic. J. Phys. I 2(12), 2221–2229.
Ngoduy, D., 2012. Application of gas-kinetic theory to modelling mixed traffic of manual and adaptive cruise control vehicles. Transportmetrica Part A 8(1), 43–60.
Ngoduy, D., 2013. Platoon-based macroscopic model for intelligent traffic flow. Transportmetrica B 1(2), 153–169.
Payne, H.J., 1971. Models of freeway traffic and control. In: Mathematical Model of Public Systems, Simulation Council Proc. La Jola California, 1, pp. 51–61.
Rahmani, M., Koutsopoulos, H.N., Jenelius, E., 2017. Travel time estimation from sparse floating car data with consistent path inference: a fixed point approach. Transp. Res. Part C 85, 628–643.
Ramezani, M., Geroliminis, N., 2012. On the estimation of arterial route travel time distribution with markov chains. Transp. Res. Part B 46, 1576–1590.
Rascle, M., 2002. An improved macroscopic model of traffic flow: derivation and links with the lighthill-whitham model. Math. Comput. Model 35, 581–590.
Richards, P.I., 1956. Shock waves on the freeway. Oper. Res. 4, 42–51.
Roe, P.C., 1981. Approximate riemann solver, parameter vectors, and difference schemes. J. Comput. Phys. 43, 357–372.
Shui, H.S., 1998. TVD scheme. In: Shui, H.S. (Ed.), Finite Difference in One-dimensional Fluid Mechanics. National Defense: Beijing, pp. 333–355. In Chinese.
Smirnova, M.N., Bogdanova, A.I., Zhu, Z.J., Smirnov, N.N., 2016. Traffic flow sensitivity to visco-elasticity. Theor. Appl. Mech. Lett. 6, 182–185.
Smirnova, M.N., Bogdanova, A.I., Zhu, Z.J., Smirnov, N.N., 2017. Traffic flow sensitivity to parameters in viscoelastic modelling. Transportmetrica B 5(1), 115–131.
Tao, W.Q., 2001. Numerical Heat Transfer. Xian Jiantong University Press, Xi'an, pp. 195–251. In Chinese.
Tordeux, A., Roussignol, M., Lebacque, J.P., Lassarre, S., 2014. A stochastic jump process applied to traffic flow modelling. Transportmetrica A 10(4), 350–375.
van Lint, J.W.C., Hoogendoorn, S.P., van Zuylen, H.J., 2005. Accurate freeway travel time prediction with state-space neural networks under missing data. Transp. Res. Part C 13, 347–369.
Whitham, G.B., 1974. Linear and Nonlinear Waves. Wiley, NewYork.
Wu, C.H., Mo, J.M., Lee, D.T., 2004. Travel-time prediction with support vector regression. IEEE Trans. Intell. Transp. Syst. 5(4), 276–281.
Xie, Z.M., Zhu, Z.J., Hu, J.J., 2006. Numerical study of mixed freeway traffic flows. Commun. Numer. Methods Eng. 22 (1), 33–39.
Xu, R.Y., Zhang, P., Dai, S.C., Wong, S.C., 2007. Admissibility of a wide cluster solution in anisotropic higher-order traffic flow models. SIAM J. Appl. Math. 68(2), 562–573.
Yildirimoglu, M., Geroliminis, N., 2013. Experienced travel time prediction for congested freeways. Transp. Res. Part B 53, 45–63.
Zhang, H.M., 2003. Driver memory, traffic viscosity and a viscous vehicular traffic flow model. Transp. Res. Part B 37, 27–41.

Zhang, P., Wong, S.C., Dai, S.Q., 2009. A conserved higher order aniso-tropic traffic flow model: description of equilibrium and non-equilibrium flows. Transp. Res. Part B 43(5), 562–574.
Zhu, Z.J., Wu, T.Q., 2003. Two-phase fluids model for freeway traffic and its application to simulate the evolution of solitons in traffic. ASCE, J. Transp. Eng. 129, 51–56.
Zhu, Z.J., Yang, C., 2013. Visco-elastic traffic flow model. J. Adv. Transp. 47, 635–649.
Zhu, Z.J., Chang, G.L., Wu, T.Q., 2004. Numerical analysis of freeway traffic flow dynamics under multiclass drivers. Transp. Res. Record.: J. Transp. Res. Board 1852, 201–219.